Fisheries and Oceans Canada | Pêches et Océans Canada
Ecosystems and Oceans Science | Sciences des écosystèmes et des océans

**Canadian Science Advisory Secretariat (CSAS)**

**Research Document 2021/068**

**Quebec Region**

# Linking interannual variations of capelin abundance indices in the Gulf of St. Lawrence to environmental proxies of bottom-up regulation of cohort strength

Caroline Lehoux, Stéphane Plourde, Jean-Martin Chamberland and Hugues Benoît

Fisheries and Oceans Canada
Maurice-Lamontagne Institute
850, Route de la Mer
Mont-Joli, Quebec Canada G5H 3Z4

February 2022

Canada

**Foreword**

This series documents the scientific basis for the evaluation of aquatic resources and ecosystems in Canada. As such, it addresses the issues of the day in the time frames required and the documents it contains are not intended as definitive statements on the subjects addressed but rather as progress reports on ongoing investigations.

**Published by:**

Fisheries and Oceans Canada
Canadian Science Advisory Secretariat
200 Kent Street
Ottawa ON K1A 0E6

http://www.dfo-mpo.gc.ca/csas-sccs/
csas-sccs@dfo-mpo.gc.ca


ISSN 1919-5044
ISBN 978-0-660-41158-3 Cat. No. Fs70-5/2021-068E-PDF

**Correct citation for this publication:**

Lehoux, C., Plourde, S., Chamberland, J.-M., and Benoît, H. 2022. Linking interannual variations of capelin abundance indices in the Gulf of St. Lawrence to environmental proxies of bottom-up regulation of cohort strength. DFO Can. Sci. Advis. Sec. Res. Doc. 2021/068. iv + 51 p.

***Aussi disponible en français :***

*Lehoux, C., Plourde, S., Chamberland, J.-M., et Benoît, H. 2022. Relier les variations interannuelles des indices d'abondance du capelan dans le golfe du Saint-Laurent aux indicateurs environnementaux de la régulation ascendante de la force des cohortes. Secr. can. des avis sci. du MPO. Doc. de rech. 2021/068. iv + 58 p.*

## TABLE OF CONTENTS

## ABSTRACT

In this study, we applied a conceptual model relating capelin cohort strength to bottom-up processes using newly developed capelin abundance indices and descriptors of physical and biological oceanographic conditions in the Gulf of St. Lawrence (GSL). The main objective of the analyses was to provide evidence that abundance indices estimated from bottom-trawl surveys in the GSL track some of the variation expected from environmental conditions known to control variations in capelin cohort strength on the eastern Newfoundland shelf. In addition, we sought to improve our understanding of environmental drivers of capelin dynamics and productivity in the GSL over the last 3 decades. Our approach included (1) the development of a capelin larval abundance indices considered as a potential explanatory variable in the conceptual (2) analyses aimed at documenting the links between physical oceanographic conditions, spring bloom and *Calanus* dynamics, and capelin body condition in the GSL, and (3) multivariate non-linear models relating capelin abundance indices in different sub-regions of the GSL with environmental indices or capelin condition used as proxies of capelin survival potential. Our results showed that the seasonal phenology and June abundance of *Calanus hyperboreus* was associated with the ice and spring bloom dynamics, while the phenology and abundance of *C. finmarchicus* was mostly associated with sea-surface temperature (SST) indices in spring and early summer. High capelin body condition (Kn) in June was related to either early ice retreat or associated high *C. hyperboreus* abundance and early development timing, while high Kn in August-September was observed in years with a late timing of *C. finmarchicus* population development or a high *C. finmarchicus* abundance and SST during summer. Variations in capelin abundance indices were generally associated with variations in Kn in June and/or in August-September or their environmental proxies during the first 1-2 years of life in capelin, but not to capelin larval abundance indices. Timing of ice retreat was selected in 5 out of 6 models whereas proxies of Kn in August-September were selected in 3 of 4 models. Our results therefore identified sea ice dynamics (late winter-early spring) or SST (late spring-summer) as potential key drivers of *Calanus* species dynamics and capelin condition, confirming the bottom-up hypothesis implicitly considered in the predictive model of capelin biomass on the eastern Newfoundland shelf. Our results also confirmed that capelin abundance indices derived from bottom-trawl surveys in the GSL generally track variation in abundance expected from known bottom-up processes regulating capelin's cohort strength.

# 1. INTRODUCTION

Capelin stock assessment in the Gulf of St. Lawrence (NAFO 4RST) is considered as data-poor (DFO 2018). Assessments prior to 2021 were based on limited commercial fishery and biological data (sex, body length), with no accepted abundance indices available for this stock (Chamberland et al. 2022a).

For the 2021 assessment, Chamberland et al. (2022b) designed a set of analyses aimed at determining how capelin physical habitat preferences and demersal fish predation risk would affect capelin catches in bottom-trawl surveys in the southern and northern Gulf of St. Lawrence (sGSL and nGSL here after). Results showed that (1) capelin was mostly caught in areas where bottom temperature corresponds to capelin preferred temperature (<3$^{o}$C, corresponding to bottom depths 50-175 m), (2) catch level in this preferred capelin thermal habitat varied accordingly with the prediction that capelin would be more available to the bottom trawl during daytime when it is closer to the bottom, and (3) demersal fish predation risk indices explained <1.5% of the variation in catches. Additionally, size frequency distribution of capelin suggested that 2-3 year old and 1-2 year old capelin dominate capelin catches in the nGSL and sGSL bottom surveys respectively. Abundance indices were calculated while considering capelin thermal (depth) habitat preferences. These indices showed considerable medium-term variations (but only moderate interannual variation) during the 1990-2020 period, with some coherence between the sGSL and nGSL(Chamberland et al. 2022b).

Lewis et al. (2019) explored a variety of hypothesis to explain interannual variations in 2 year-old capelin abundance estimated during the Spring acoustic survey in 3KL. They found that 2 year-old abundance in the Spring (t0) was best predicted by the abundance of emerging larvae two years prior (t0-2), body condition of 1 year old capelin during the previous fall (t0-1) and the timing of ice retreat (t0) (Lewis et al. 2019). The last two predictors were interpreted as proxies of capelin survival potential during its second winter of life and the following spring. Lewis et al. (2019) implicitly hypothesized that the timing of ice retreat would control the timing of the spring phytoplankton bloom and *Calanus* abundance and phenology, and therefore capelin prey availability and survival in spring (Dalpadado and Mowbray 2013; Buren et al. 2014; Mullowney et al. 2016).

Pelagic fish abundance indices derived from bottom trawl surveys are considered to be highly uncertain because this gear is considered a poor sampler of pelagic fish for various reasons (O'Driscoll et al. 2002, Mowbray 2002, McQuinn 2009). However, the strong link between capelin cohort strength (abundance) and bottom-up processes described in 3KL offers a framework to perform a first order validation of the abundance indices derived from DFO's bottom trawl surveys in the GSL. In this study, we developed a conceptual model of survival (cohort strength) for 4RST capelin using newly developed capelin abundance indices in the GSL derived from Chamberland et al. (2022b) in order to (1) provide evidence that abundance indices estimated from bottom-trawl surveys in the GSL meaningfully tract some of the variation in abundance expected from varying environmental conditions known to control cohort strength of 3KL capelin, and (2) improve our understanding of environmental drivers of capelin dynamics and productivity in the GSL over the last 3 decades. The capelin survival model was largely inspired from the one developed for 3KL capelin (Lewis et al. 2019) but adapted to the data and ecosystem features specific to the GSL. We first described the bottom-up processes in the lower food web hypothesized to control capelin survival by linking sea ice conditions, plankton dynamics and capelin body condition in the different regions in the GSL. We then adapted the conceptual model of capelin survival and cohort strength in 3KL and tested whether interannual variations in capelin abundance observed between 1990 and 2020 in the GSL were associated with bottom-up processes known to regulate capelin survival and cohort strength. Our analyses

represent an application of an Ecosystem Approach to Fisheries Management (EAFM) with the overachieving goal of improving the current knowledge routinely available to the 4RST capelin stock assessment in support to the science advice.

# 2. METHODS

## 2.1. CAPELIN STOCK AND ENVIRONMENTAL INDICES

### 2.1.1. Abundance indices

Abundance indices used in these analyses were derived from the nGSL (August) and sGSL (September) multidisciplinary bottom-trawl surveys 1990-2020 (Figure 1). These surveys mainly target demersal fishes but detailed analysis showed that capelin caught in the bottom trawl were mostly associated with bottom temperatures ranging from -1$^{o}$C to 3.3$^{o}$C typical of the Cold Intermediate Layer (CIL, Galbraith et al. 2020) and with catches following the expected pattern associated with capelin diel vertical migrations (larger catches during daytime when capelin are close to the bottom) (Benoît and Swain 2003; Chamberland et al. 2022b). Therefore, capelin abundance indices used in our analyses were computed for the North-West and North-East GSL (respectively nwGSL and neGSL hereafter, Figure 2) using catches in tows with bottom temperature < 3.3°C and standardized as if they were caught during the day. More specifically, capelin abundance per tow was modeled with a negative binomial glm using year (as a factor) * nGSL region interaction, day/night coded as a binary variable, as well as an offset accounting for log towed surface area. Abundance indices (mean number per tow) for the nwGSL and neGSL were then predicted for each year for a standard tow (15 minutes at 3 knots with trawl opening width of 16.94m) performed during the day. Capelin sGSL abundance indices used in the present study were those computed with the negative binomial model with annual stratum effect following a first-order autoregressive process (NB AR(1) model) in Chamberland et al. (2022b). The use of regional abundance indices (nwGSL, neGSL and sGSL) was motivated by regional differences in environmental conditions (Blais et al. 2019) as well as allowing finer scale capelin – environment relationships. Therefore the abundance indices for the nw and neGSL used in this manuscript differ from Chamberland et al. (2022b) because they did not consider the regional differences in abundance in time for the preparation of this document. Nevertheless, the abundance indices used in this manuscript show the same general pattern of variability as they are correlated to the abundance index developed for the whole nGSL by Chamberland et al. (2022b) (neGSL: r=0.52, p=0.03, nwGSL: r=0.46, p=0.01, nGSL; r=0.58, p=0.0007).

### 2.1.2. Larval abundance index

In their model of 3KL capelin cohort strength, Lewis et al. (2019) used a seasonally-integrated abundance index of emerging capelin larvae from a reference bay considered representative of capelin spawning in the region (Murphy et al. 2018). In order to apply that model to capelin in the GSL, we developed a larval abundance index using data collected during a synoptic egg and larval survey conducted in June in the sGSL since 1983 (no surveys in 1995 or 1997). Capelin larvae are captured each year during this survey is generally undertaken during or slightly after the peak in capelin beach spawning in the region, implying that the survey could potentially provide abundance indices for locally produced young larvae (Grégoire et al. 2014, Chamberland et al. 2022a). Briefly, a grid of 65 stations was sampled with 333 µm mesh Bongo nets (61 cm) using double oblique tows in the upper 50 m of the water column for a minimum of 10 min at a ship speed of ~2.5 kts. In order to (1) validate that the survey sampled mostly small/young larvae close to their emergence timing and (2) account for the potential effects of

variations in the timing of the survey and in the timing of emergence of capelin larvae, we measured the lengths of 10 capelin larvae from a subset of stations where larvae occurred. From these measurements we calculated the station mean larvae length from which we estimated the number of days since emergence using growth curves estimating that capelin larvae grew between 0.2-0.35 mm per day (Jacquaz et al. 1977) and estimated the number of days since emergence assuming capelin larvae hatched at 5 mm. The hatching date was defined as the difference in days between the sampling date and the number of days since hatching. For stations where no larvae were measured, emergence dates were assigned to each station following a hierarchal approach using: (1) the distance-weighted mean hatching date of the three closest stations within 100 km, or (2) mean annual hatching date for stations more than 100 km away from stations with length measurements, or (3) mean hatching date over the 1983-2019 period during years with no length measurements (1991,1992,1994,1999 and 2012) (Appendix 1 Figure A.1.1).

Larval abundance (N $m^{-2}$) was standardized using a Generalized Additive Model (GAM) with a negative binomial distribution and log link. The goal of this standardization was to obtain abundance indices as if the survey was consistently undertaken during the peak of larval emergence. We used a tensor product smooth to model the spatial distribution of capelin larvae for each year and the tensor product interaction and main effect of the sampling date and the larvae emergence date (day of year) at each station (Wood 2006). We also tested the effect of the number of days since emergence as a substitute for hatching date and other less complex models with different combinations of these variables. The formulas of each models tested are presented in Table 1. The model with the lowest AIC was selected and the fitted values were simulated to verify the dispersion and the proportion of zero values in 1000 simulated datasets (Zuur and Ieno 2016). The homogeneity of the residuals was verified visually. Temporal and spatial correlation of the residuals were examined with the acf function and a variogram respectively to comply with the assumption of residuals independency. Using the selected model, we predicted the abundance at each station of the grid for each year using the 1983-2019 mean sampling (day of year = 170) and emergence date (day of year = 160). The mean standardized abundance (N $m^{-2}$) for each year is used as the larval index. Stations where larvae were absent were not standardized before calculating the annual mean.

### 2.1.3. Condition indices

Conditions indices (Kn, Le Cren 1951) were calculated from biological samples collected during the commercial fishery and the nGSL (August) and sGSL (September) bottom-trawl surveys. For commercial fishery samples, GLMs with a Gaussian family and log link were fitted using Kn as response variable and year, month and fishing gear as factors (Chamberland et al. 2022a). Kn from commercial fisheries was standardized by predicting the annual mean for each sex and region by fixing factors month and fishing gear to the bulk of samples, i.e. June and seiners respectively, and is referred to as “Kn June” afterward. These Kn indices were used in our models as a proxy of capelin feeding success and survival potential in the spring. For the bottom-trawl surveys (Kn August or Kn September), we used fish < 120 mm according to our objective of assessing the role of potential survival during the next winter of 1-year and 2-year old capelin (see capelin survival conceptual models M1 and M2 below). According to measurement by Hurtubise (1994) these smaller capelin would be 1-2 years old and sexual dimorphism at this size would be minimal. Therefore separate sex-specific weight-length relationships were not required (Figure 3). Inter-annual variation in Kn indices are presented in Appendix 2 (Figure A.2.1).

### 2.1.4. Environmental indices

Environmental indices were extracted from the GSL Ecosystem Matrix (Duplisea et al. 2020) This matrix contains various physical, biochemical and biological indices produced by the Atlantic Zone Monitoring Program (AZMP) and used to describe the state of the ocean on an annual basis (Galbraith et al. 2020; Blais et al. 2019). These environmental indices were selected based on their availability, putative effects on the zooplankton dynamics and capelin body condition and survival (Buren et al. 2014; Mullowney et al. 2016; Murphy et al. 2018; Lewis et al. 2019), and local characteristics (i.e. differences in zooplankton communities between the Newfoundland shelf and the GSL) (Table 2). Physical indices were available for a longer time period (1982-2019; Galbraith et al. 2020) than zooplankton indices in general (2001-2019; Blais et al. 2019). Selected physical indices were sea surface temperature (SST) in June and May-August, the spring timing (week of the year when SST warms up to 10°C) and timing of ice retreat (last day of ice). The timing of the onset of the spring phytoplankton bloom in different regions in the GSL was included to describe the implicit link assumed by Lewis et al. (2019) between the timing of ice retreat, onset of the bloom and zooplankton dynamics (1998-2019; Blais et al. 2019). Zooplankton indices included abundance of key copepod prey of capelin larvae (*Pseudocalanus*; Murphy et al. 2018) and 1-2 year old capelin (*C. finmarchicus*, *C. hyperboreus*; Vesin et al. 1981; Ménard 1998; Astthorsson and Gislason 1997; Orlova et al. 2009; Dalpadado and Mowbray 2013) in different seasons (June, July-December), as well as population development indices of *Calanus* species used as an indicator of their timing in the spring (Table 2). Environmental indices were computed for 5 different regions in the GSL (Figure 2) and were combined as followed to match capelin body condition and abundance survey data: region 1 (North-West GSL: nwGSL), 2, 3 and 4 (North-East GSL: neGSL) and 5 (Southern GSL: sGSL). The annual region-specific averages were weighted by the surface area of each Ecosystem Approach (EA) region to derive a single annual estimate (Duplisea et al. 2020). Time series of the environmental indices are presented in Appendix 2 (Figure A.2.2).

## 2.2. MODELS

### 2.2.1. Modelling approach, model selection and validation

The GAMs were chosen over GLMs because preliminary analysis showed potential for non-linear responses of independent variables to some predictors. GAMs followed a Gaussian distribution and a log link function. Correlations and relationships were verified among predictors and correlated predictors (> 0.6) were not included simultaneously in models. Outliers were investigated by dotplots and we removed Kn > 1.3 and < 0.75 which were also associated with small sample size. All models considered a maximum of 3 predictor variables and were tested in order to minimize potential of overfitting and evaluated according to their AIC corrected for small sample size (AICc, Burnham and Anderson 2002; Hurvich and Tsai 1989). The basis dimension (k) was set to a maximum of 3 to avoid multi-modal unrealistic relationships and overfitting. The $R^2$ between predictions and observations and the deviance explained were calculated and model robustness was evaluated using a bootstrap and leave-one-out cross-validation (jackknife) (Guisan and Zimmermann 2000). The bootstrap consisted of resampling predictors and refitting the model 1000 times. The deviance explained was calculated for each iteration and the deviance explained by the model was compared to this distribution. The deviance explained by the selected model should be higher than the 95th percentile of the simulated datasets for the model to be retained. Each model was also tested using a jackknife procedure. For each model, we removed one year at a time, fitted the model and predicted the value. The predicted values were compared to the observed values and the Pearson's correlation coefficient (r) between observations and predictions was calculated. The final selected model had the lowest AICc ($\Delta$ <2), was significant (< 0.05) in the bootstrap and was

robust against missing years (jackknife r $\Delta$ < 0.1). When two models had similar performances on all indicators, the most parsimonious model was selected. Model residuals were checked for temporal autocorrelation using the acf function in R. All analyses were done in R v. 4.0.2 (R Core Team 2020) and GAMs were fitted using the mgcv package (Wood 2017). Conditions of applications (homogeneity, normality and observed against fitted values) were verified visually.

### 2.2.2. Kn

GAMs were fitted for capelin Kn to (1) describe the links between capelin body condition and bottom-up processes (sea ice and plankton dynamics) and (2) identify key environmental proxies for Kn that can be used in capelin abundance models. The expected effect (hypothesis) of these predictors on capelin Kn are described in Table 2. Kn in June was related to environmental condition in spring, whereas Kn in August (nGSL) or September (sGSL) was related to environmental indices from spring to late summer. We adopted a stepwise approach when considering environmental predictors of different categories: (1) physical indices representing the longest time series (1983-2019) and (2) physical and zooplankton indices corresponding to the shorter time series (2001-2018). *C. finmarchicus* and *C. hyperboreus* abundance (June, July-September) and development indices (timing) in June were considered as these species generally represent a large proportion of the diet of 1-year and 2-year old capelin (Vesin et al. 1981; Dalpadado and Mowbray 2013).

### 2.2.3. Abundance

According to the length at age data from 1984-1993 GSL commercial samples (Hurtubise 1994), capelin from the sGSL bottom trawl survey would be mostly 1 and 2 years old individuals, those from the nGSL bottom trawl survey would be mostly 2 and 3 years old individuals, while the commercial fishery in the sGSL and nGSL would mostly capture 3+ years old capelin (Figure 3) (Chamberland et al. 2022b).

The uncertainty associated with capelin age structure in the annual abundance indices was accounted for in our study by developing different abundance model structures. Following Lewis et al. (2019), the first conceptual model (see below and Figure 4 for predictors) hypothesized that capelin abundance dominated by 2 year old individuals (models M2) would vary as a function of the following additive processes:

*(M2) Capelin abundance $_{(t0)}$ = larval production/ survival $_{(t-2)}$ + capelin (1-year old) winter survival $_{(t-1)}$ + capelin (2-years old) post-winter survival $_{(t0)}$*

In the second model, capelin abundance dominated by 3-years old individuals (models M3) would vary as a function of:

*(M3) Capelin abundance $_{(t0)}$ = larval production/ survival $_{(t-3)}$ + capelin (1-year old) winter survival $_{(t-2)}$ + capelin (2-years old) post-winter survival $_{(t-1)}$*

Finally, the third model hypothesized that capelin abundance dominated by 1-year old individuals (model M1) individuals would vary as a function of:

*(M1) Capelin abundance $_{(t0)}$ = larval production/ survival $_{(t-1)}$ + capelin (1-year old) post-winter survival $_{(t0)}$*

Model M2 (catches dominated by 2-year old) was applied to abundance indices in the neGSL, nwGSL, and sGSL. Model M3 (catches dominated by 3-years old) was applied to the neGSL and nwGSL indices. Model M1 (catches dominated by 1-year old) was only applied to the sGSL.

The set of predictors associated with each model term are presented in Figure 4 and their expected effect (hypothesis) on capelin Kn and survival are detailed in Table 2. According to

models, high (low) survival during 2 or 3 successive key events occurring during the first 1-2 years of life of each cohort would result in high (low) abundance indices, while variations in survival among those events would produce moderate abundance. We used the abundance of *Pseudocalanus* spp. in July-October at the Shediac Valley station (sGSL) and Rimouski station (nwGSL) as a proxy for larval survival (Murphy et al. 2018). Kn in Fall and Spring were respectively used as a proxy for capelin potential survival during winter (mainly reproductively immature capelin < 120 mm) or in spring (mainly reproductively mature capelin) (Buren et al. 2014; Lewis et al. 2019).

Since Kn time series are discontinuous (no samples or n too small, see Chamberland et al. 2022a), their use as predictors for survival resulted in variable effective time series shorter than those of physical environmental indices. We therefore also considered environmental predictors of Kn (see Figure 4 and section 3.2.1) with the physical indices time series being longer than the zooplankton time series (Table 2). The different length of the time series led to a hierarchical approach of model testing where predictors were removed from the model if their effect did not support the associated hypothesis (Table 2) and/or did not improve the jackknife relative to the longer time series. The longer time series were preferred if the difference between the $R^2$ or jackknife correlation between the longer and smaller time series was less than 0.1. GAMs were fitted and validated using a similar approach to the models fitted for Kn except that the formulas were hypothesis-based rather than allowing combinations of variables. Capelin abundance was log-transform prior to model fitting. Hypotheses never included more than 4 variables simultaneously to avoid overfitting due to the short time series.

# 3. RESULTS

## 3.1. CAPELIN STOCK AND ENVIRONMENTAL INDICES

### 3.1.1. Larval abundance index

Larvae length varied between 2 mm and 19.7 mm with a dominant mode of larvae smaller than 10 mm in most years (Figure 5 A).The average day of year of the mackerel egg survey in the sGSL was 171 (sd=5.6) while the mean estimated hatching day was 160 (sd=8.2) (Figure 5B). The GAM with the lowest AIC included the spatial effect and the main effects (and their interaction) of the sampling and estimated hatching date (Table 1). The spatial effect explained more deviance than the sampling and hatching day, but all effects were significant (confidence intervals of partial effects excluded the dotted line on 0, Figure A.1.2). The selected model explained 1.3% more deviance than the spatial effect alone. The selected model assumptions were verified: the model showed no sign of overdispersion, predicted a number of absence similar to the data and the residuals showed no sign of temporal or spatial autocorrelation or heterogeneity. The spatial effect showed that the larval distribution varied among years, although higher larvae abundances were generally observed near the Chaleur Bay (Appendix 1, Figure A.1.2). Larval abundance was positively and negatively related to sampling and hatching day respectively. However, their interaction term indicated that the higher larval abundances occurred when the difference between the two dates ranged from 10 to 20 days, suggesting that lower than expected larval abundances were associated with either a sampling day too close to hatching day (probably because a large fraction of eggs did not yet hatch) or too late after hatching (probably due to cumulative mortality during larval development) (Appendix 1, Figure A.1.3). Larval abundance was generally scaled down by the model adjustment between 1983 and 2006, but scaled up since the survey occurred earlier since 2009 (Appendix 1, Figure A.1.4). Some very high standardized abundance indices were estimated early (1986, 1990) and late (2017-2019) over the time series that were superimposed over a pattern characterized by a

general decrease between the early 1980's and mid 1990's followed by a period of generally higher values centered during the late 2000's (Figure 6). The high larval abundances observed in 2018, 2019 could only be partially explained by the timing of the survey. The 2018-2019 standardized values remain 3-10 times larger than all values in the time series.

### 3.1.2. Environmental indices

Pearson's correlation coefficient (r) among environmental indices are described in this section. The timing of the bloom was positively correlated with the timing of ice retreat in all regions, although the correlation was not statistically significant in the neGSL (r= 0.48, *p-value*=0.2) (Figures 7,8,9). This result generally supports the hypothesis that the timing of sea ice retreat controls the timing of the onset of the phytoplankton bloom in the GSL. The spring timing (first week with SST = 10$^{o}$C) was negatively correlated with SST in May-August, indicating that an earlier (later) increase of SST resulted in higher (lower) average SST during the spring-summer (Figures 7,8,9). In all regions, the spring timing was not correlated with the timing of sea ice retreat, indicating that these two processes are controlled by different environmental forcing (Figures 7, 8, 9; Galbraith et al. 2020).

In the neGSL (Figure 7), the *C. hyperboreus* development index in June was negatively correlated with the timing of ice retreat (-0.68, p=0.0006), i.e. the development of *C. hyperboreus* new generation was more advanced with an earlier timing of ice retreat (and onset of the phytoplankton bloom). *C. hyperboreus* abundance in June was negatively correlated with its development index (-0.45, p=0.06). The *C. finmarchicus* development index was correlated with the spring timing (0.60, p=0.02) but not with the timing of ice retreat. The later surface waters warmed to 10$^{o}$C, the later the timing of population development was, *C. finmarchicus* abundance was positively correlated to its development index (0.63, p =0.006).

In the nwGSL (Figure 8), *C. finmarchicus* abundance and development index in June were correlated (0.58, p=0.01). The *C. hyperboreus* abundance in June and in July-September were also positively correlated (0.89, p<0.0001).

In the sGSL (Figure 9), the *C. hyperboreus* development index in June was negatively correlated to the timing of ice retreat (-0.47, p=0.07). *C. hyperboreus* abundance was correlated to its development index (0.51, p=0.02), indicating that higher abundance was associated with an earlier development. The *C. finmarchicus* development index was positively correlated to the spring timing (0.52, p=0.047).

In summary, the onset of the spring bloom in the GSL was generally associated with the timing of ice retreat. Our results also indicated that *C. hyperboreus* timing and abundance in June was associated with the ice and spring bloom dynamics, while the timing and abundance of *C. finmarchicus* was more associated to SST-related environmental indices.

## 3.2. MODELS

### 3.2.1. Kn

In the neGSL, the best model for Kn in June included SST in June and the timing of ice retreat (Figure 10 and Table 3). This model had the lowest AIC but a low $R^2$ (0.18) with a poor performance during the jackknife and bootstrap procedures. It was nevertheless presented because the relationship between Kn and the timing of ice retreat was coherent with the hypothesis that colder spring combined with an early ice retreats would be favorable to Kn in June. SST and the timing of ice retreat showed a negative effects on Kn but the effect of SST was not significant. However, the model had a limited scope and should be considered with caution.

In the nwGSL (Table 4), no model was selected for Kn in June (Appendix 4 Table A4.3). For Kn in August (whole nGSL), a model including a positive effect of the *C. finmarchicus* development index in June ($R^2$ = 0.5) was selected based on its lower AIC and performance in the bootstrap and jackknife procedures (Figure 11, Table 4, Table A.4.3). This model suggests that a later timing of *C. finmarchicus* population development in late spring and early summer would be beneficial for capelin Kn in August.

In the sGSL (Table 5), the timing of ice retreat showed again a significant negative effect on Kn in June. However, similarly to the neGSL, the model was not significant according to the bootstrap test (Table A.4.4). However, a model considering zooplankton indices was selected. Kn in June was negatively related to the *C. hyperboreus* development timing (Figure 12 and Table 5). This model had an adjusted $R^2$= 0.78 and performed well both in the bootstrap and jackknife procedures. This model was selected even if its AIC was higher because other models with lower AIC were likely overfitted. This effect could also be related to abundance as the *C. hyperboreus* development index and abundance were correlated (Figure 9). Kn in September was negatively related to SST in May-August (1990-2019) (Figure 13) or positively related to *C. finmarchicus* abundance in July-September (1999-2019) (Figure 14), with the later showing an improved adjusted $R^2$ = 0.50 and performance of the Jackknife procedure over the model that included only SST (Table 5).

In summary, high Kn in June was related to an early timing of ice retreat or to high *C. hyperboreus* abundance and early development timing. High Kn in August-September was associated with either a late timing of *C. finmarchicus* population development or a high *C. finmarchicus* abundance and SST during summer (July-September).

### 3.2.2. Abundance

The larval abundance indices derived from the survey in June in the sGSL showed no significant effect in any of the best M1, M2 and M3 models (Tables 3-5), neither in any of the models built along our analytical stepwise procedure (Appendix 4).

In the neGSL, the best abundance model assumed that 3-year old capelin dominated in the catches (M3) and included Kn in June at age-1 and the timing of ice retreat at age-2 as explanatory variables (Table 3). The timing of ice retreat showed a dome-shape effect indicating that extreme years were unfavorable for age-1 capelin survival in spring whereas the positive effect of Kn in June would reflect a greater survival of age-2 capelin (Figure 15). The performance of the model assuming that 2–year old individuals were dominant (M2) was only slightly lower with the same explanatory variables (Table 3). Both models showed that years with high (low) capelin abundance were associated with positive (negative) effects of explanatory variables, i.e. during the first two years of capelin life (Figure 15, Figure A.3.1).

In the nwGSL, the best abundance model also assumed that 3-years old capelin dominated in the catches (M3) and included Kn in June at age-1 (Table 4). The effect was mostly positive and the model performed well at predicting some of the most extreme low capelin abundance as well as the contrasting period of predominantly high (2007-2012) and low (2013-2019) capelin abundance (Figure 16). The model assuming that 2–year old individuals were dominant (M2) included a positive and significant effect of *C. finmarchicus* abundance in July-September at age-1, suggesting that good summer feeding condition could favor capelin survival during the following winter (Table 4, Figure A.3.2). However, timing of ice retreat corresponding to capelin survival at age-2 was not significant and the overall model performance was lower (Table 4).

In the sGSL, the best abundance model assumed that 2-year old capelin dominated in the catches (M2) and included SST May-August at age-1 (positive effect) and the timing of ice retreat at age-2 (negative effect) as explanatory variables (Table 5, Figure 17). SST May-August

was associated to higher Kn in September (as a proxy for a greater survival of age-1 individuals during next winter) while an earlier timing of ice retreat would promote higher survival of age-2 capelin during the following spring (Table 5). The model predicted well the low capelin abundance in the early 1990s, the higher abundance over the following decade with maximum values around 2010, but underestimated abundance in 2011-2015 (Figure 17). The best model assuming that 1–year old individuals were dominant (M1) only included the timing of ice retreat at age-1 as explanatory variable, but with a performance substantially lower than the M2 model (Table 5, Figure A.3. 1).

In summary, variations in capelin abundance indices in the bottom-trawl surveys were associated to variations in Kn (as a proxy of survival) in June and/or in August-September or to their environmental proxies. Timing of ice retreat was selected in 5 out of 6 models whereas proxies of Kn in August-September were selected in 3 of 4 models in the sGSL and nwGSL. Models fits were better for M3 models in the neGSL and nwGSL and for models M2 in the sGSL. M2 model in the sGSL showed the best performance among all models. Therefore, our results largely support the conceptual model predicting that capelin abundance (cohort strength) would be associated with variations in survival driven by bottom-up processes during its first 1-2 years of life.

## 4. DISCUSSION AND CONCLUSION

Our results support the hypothesis that environmental and biological conditions known to regulate capelin survival and cohort strength (Lewis et al. 2019) explain some of the variation in capelin abundance indices from bottom trawl surveys in the GSL. Our results also identified correlation between sea ice dynamics (late winter-early spring) or SST (late spring- summer) and *Calanus* species dynamics and capelin condition, supporting the bottom-up hypothesis implicitly assumed in the predictive model of capelin biomass in 3KL (Buren et al. 2014; Lewis et al. 2019). Variations in capelin abundance indices were mainly associated with variations in Kn in June and/or in August-September or their environmental proxies, supporting the conceptual hypothesis that capelin abundance at age 2 is largely associated with variations in survival occurring at age-1 and/or age-2 (Lewis et al. 2019). According to our results with models M2 and M3 and our description of species-specific *Calanus*-environment dependencies, good environmental conditions in summer-fall at age-1 (good Kn and survival during the next winter) have to precede similarly favorable environmental conditions at age-2 during the next spring (good Kn and survival) to produce a strong cohort (high abundance).

A correlation between the timing of ice retreat and the onset of the spring bloom was observed in most regions. Our results also indicated that *C. hyperboreus* timing and abundance was associated with the timing of sea ice retreat with an earlier (later) timing of ice retreat (with its effect on the timing of the spring bloom) leading to an earlier (later) timing of *C. hyperboreus* population development. The timing and abundance of *C. finmarchicus* was not associated with the timing of ice retreat but rather to post-bloom environmental conditions (spring timing, SST in June) with an earlier (later) spring warming resulting in an earlier (later) timing of *C. finmarchicus* population development. These species-specific links with environmental conditions during the spring-early summer are conformed with their respective life cycle strategy. *C. hyperboreus* is a capital breeder reproducing in deep waters in winter with its offspring taking advantage of the spring bloom to rapidly develop in surface layer (0-100 m) and enters diapause in late spring/early summer (Plourde et al. 2003). *C. finmarchicus* is an income breeder with a period of active population development/growth in the surface layer during summer and an entry in diapause in late summer (Plourde et al. 2001; Blais et al. 2019). In all regions, the lack of correlation between the timing of sea ice retreat and spring timing indicate

that *C. hyperboreus* and *C. finmarchicus* dynamics are somewhat decoupled and potentially influenced differently during any given year.

The fact that Kn in June was related to the timing of ice retreat or to *C. hyperboreus* indices while Kn in August-September was associated with *C. finmarchicus* dynamics or seasonally-averaged SST (May-August) matched the general *Calanus* seasonal dynamics described above. *C. hyperboreus* is frequently ranked first, second or third in number in the stomach content of capelin captured in spring and early summer (Vesin et al. 1981; Ménard 1998; Astthorsson and Gislason 1997; Orlova et al. 2009; Dalpanado and Mowbray 2013). Because of its much larger body size and high lipid content, it could therefore represent a dominant contributor of capelin's energy intake (Lehoux et al. 2020). We therefore propose that 1-2 year old capelin survival after winter (proxy = Kn June) would be mainly regulated by the sea ice- *C. hyperboreus* dynamics and the presence of this species in surface layer in the spring. On the other hand, 1 year old capelin survival during the following winter (proxy = Kn August-September) would be mostly driven by summer SST- *C. finmarchicus* dynamics and the presence of this species in the surface layer in summer. *Calanus* species-specific seasonal vertical distribution patterns and presence in the surface layer likely drives their availability for capelin foraging (Plourde et al. 2019; Aarflot et al. 2020). Diapausing *C. hyperboreus* are usually observed deeper than 250 m and therefore capelin's optimal thermal habitat in the nGSL, while *C. finmarchicus* generally overwinter in colder waters at 150 m to 175 m deep (Plourde et al. 2019). The key role of both *C. hyperboreus* (spring) and *C. finmarchicus* (summer) supported by our results differs from the conceptual model developed for capelin in 3KL, where only *C. finmarchicus* was considered (Buren et al. 2014; Lewis et al. 2019).

Contrary to the nGSL, the shallow depth (< 100 m) in the sGSL could make *C. hyperboreus* available for capelin foraging even after its entry into diapause in late spring as suggested by models showing a significant positive effect of *C. hyperboreus* abundance (June) on capelin's Kn in September (Table A.4.3). The vertical distribution of diapausing *C. hyperboreus* is constrained by bottom depth in the sGSL, which increases its density and availability for capelin's foraging compared to the nGSL (Plourde et al. 2019; Aarflot et al. 2020). Diapausing *Calanus* concentrated near the bottom in the sGSL would also be little affected by transport and have a long residence time (3-4 months) in the region (Brennan et al. 2019).

Capelin larval abundance in the sGSL did not show the expected positive association with capelin abundance indices in the sGSL and nGSL (Murphy et al. 2018; Lewis et al. 2019). Murphy et al. (2018) found that older larval densities were not related to recruitment unlike emergent larvae density. It is not possible to distinguish if the lack of relationship observed in the GSL was because our larval abundance index is a poor indicator of abundance of larvae at emergence, because processes occurring later during the first 1-2 years of life identified in our analyses are dominant in determining capelin abundance in the GSL, or if other factors affect post-larval survival. Finally, advection of larvae from the St. Lawrence estuary and nwGSL later in summer could contributes to the overall processes leading to capelin abundance during the bottom-trawl survey in September in the region (Ouellet et al. 2013).

## 4.1. SOURCES OF UNCERTAINTY

We developed a larval index based on larvae abundance in the sGSL in June. The selected GAMs showed a significant effect and interaction between sampling and hatching date supporting the need to standardize the larval index. Capelin larvae are usually concentrated in the upper 0-20 m (Courtois et al. 1982; Fortier and Leggett 1983) of the water column and can thus be subjected to substantial surface transport. The larvae length distribution during the June survey suggests that those larvae were mostly spawned in the sGSL and that transport from the nwGSL was minimal at the time of the survey (Ouellet et al. 2013). The larval index was

standardized for the timing of sampling relative to the hatching estimated from larval length and standard growth rates. Development time was assumed constant both temporally and geographically, which represents a source of uncertainty considering the potential heterogeneous environmental conditions across the sGSL (Galbraith et al. 2020). The multimodal larvae length distribution in some years indicated consecutive local spawning events or various origins of the larvae but to simplify our analysis the mean length was used to calculate development time. The effect of temperature on larvae development and estimation of hatching date could be explored in the future. We also assumed that the larval abundance in the sGSL would be a good indicator of variations in annual capelin reproductive intensity across the GSL, but this assumption remains to be validated.

Krill could represent an important prey for larger/older capelin (Dalpadado and Mowbray 2013; Orlova et al. 2010). No krill abundance time series is yet available for the GSL (or elsewhere in the eastern Canadian waters). Overall, krill biomass in much greater in the nGSL than in the sGSL with krill density being greater over the slopes (bottom depth < 175 m) of the deep channels (McQuinn et al. 2015). Not considering it as a key prey for larger/older capelin might explain the generally lower performance of models in the nGSL (nwGSL, neGSL) relative to those in the sGSL.

Throughout this exercise, we assumed that there is no active migration between regions in the GSL nor from adjacent regions. Capelin abundance was assumed to be the results of local environmental conditions and mortality. However, adult capelin length (age) distribution suggest that they leave the sGSL for the nwGSL and neGSL. The abundance measured in the nGSL could then also depend on survival events that happens in the sGSL in the first years of life and survival events that happen in the nGSL later.

Density-dependence and competition were not included in our models. Lewis et al. (2019) suggested that predation and fisheries mortality should be included in the future. However, the integration of biotic interactions can be difficult because these predators/competitors also interact and are correlated with the environment (Dormann et al. 2018).

## 5. ACKNOWLEDGMENTS

We would like to thank the capelin assessment team in the Newfoundland region (F. Mowbray, A. Adamack, K, Lewis, H. Murphy, M. Koen-Alonso) for key discussions about their capelin abundance forecasting model in late Fall 2019. We would like to thank the Quebec region capelin assessment team (Mélanie Boudreau, Linda Girard) for their dedicated work necessary to provide capelin biological data and A. Smith for preliminary analyses for modelling capelin larvae abundance indices. We also thank Marjolaine Blais, Peter Galbraith and the rest of the Quebec region Ecosystem Matrix team for their work in making environmental data easily available. Finally, we would like to thank Keith Lewis and Andrew Smith for their comments on this manuscript.

## 6. REFERENCES CITED

Aarflot, J. M., Dalpadado, P., and Fiksen, Ø. 2020. Foraging success in planktivorous fish increases with topographic blockage of prey distributions. Mar. Ecol. Prog. Ser. 644: 129–142.

Astthorsson, O. S., and Gislason, A. 1997. On the food of capelin in the subarctic waters north of Iceland. Sarsia, 82: 81-86.

Benoît, H.P., and Swain, D.P. 2003. Accounting for length and depth-dependent diel variation in catchability of fish and invertebrates in an annual bottom-trawl survey. ICES J. Mar. Sci. 60: 1297-1316.

Blais, M., Galbraith, P.S., Plourde, S., Scarratt, M., Devine, L. and Lehoux, C. 2019. Chemical and Biological Oceanographic Conditions in the Estuary and Gulf of St. Lawrence during 2018. DFO Can. Sci. Advis. Sec. Res. Doc. 2019/059. iv + 64 pp.

Brennan, C. E., Maps, F., Gentleman, W. C., Plourde, S., Lavoie, D., Chassé, J., Lehoux, C., Krumhansl, K. A., and Johnson, C. L. 2019. How transport shapes copepod distributions in relation to whale feeding habitat : Demonstration of a new modelling framework. Prog. Oceanogr. 171: 1–21.

Buren, A. D., Koen-Alonso, M., Pepin, P., Mowbray, F., Nakashima, B., Stenson, G., Ollerhead, N., and Montevecchi, W. A. 2014. Bottom-up regulation of capelin, a keystone forage species. PLoS ONE, 9: e87589.

Burnham, K. P. and Anderson, D. R. 2002. Model selection and multimodel inference: a practical information-theoretic approach. 2nd ed. New York, Springer-Verlag.

Chamberland, J.-M., Smith, A.D., Girard, L., Boudreau, M., and Plourde, S. 2022a. Capelin in the Estuary and Gulf of Saint Lawrence (NAFO 4RST) in 2018, 2019 and 2020. DFO Can. Sci. Advis. Sec. Res. Doc. 2021/075. iv + 44 p.

Chamberland, J.-M., Plourde, S. and Benoît, H.P. 2022b. Biological characteristics, factors affecting catchability, and abundances indices of capelin in the southern and northern Gulf of St Lawrence multi species bottom trawl surveys. DFO Can. Sci. Advis. Sec. Res. Doc. 2021/077. iv + 41 p.

Courtois, R., M. Simoneau, et J. J. Dodson. 1982. Interactions multispécifiques: répartition spatio-temporelle des larves de capelan (*Mallotus villosus*), d'éperlan (*Osmerus mordax*) et de hareng de l'Atlantique (*Clupea harengus harengus*) an sein de la communauté planctonique de l'estuaire moyen du Saint-Laurent. Can. J. Fish. Aquat. Sci. 39:1164-1174.

Dalpadado, P., and Mowbray, F. 2013. Comparative analysis of feeding ecology of capelin from two shelf ecosystems, off Newfoundland and in the Barents Sea. Prog. Oceanogr. 114: 97–105.

DFO. 2018. Assessment of the Estuary and Gulf of St. Lawrence (Divisions 4RST) Capelin Stock in 2017. DFO Can. Sci. Advis. Sec. Sci. Advis. Rep. 2018/037.

Dormann, C. F., Bobrowski, M., Dehling, D. M., Harris, D. J., Hartig, F., Lischke, H., Moretti, M. D., Pagel, J., Pinkert, S., Schleuning, M., Schmidt, S. I., Sheppard, C. S., Steinbauer, M. J., Zeuss, D., and Kraan, C. 2018. Biotic interactions in species distribution modelling: 10 questions to guide interpretation and avoid false conclusions. Glob. Ecol. Biogeogr. 27: 1004-1016.

Duplisea, DE. Merette, D., Roux, M-J., Benoît, H., Blais, M., Galbraith, P., and Plourde, S. 2020. gslea: the Gulf of St Lawrence ecosystem approach data matrix R-package. R package version 0.1.

Fortier, L., and Leggett, W. C. 1983. Vertical Migrations and Transport of Larval Fish in a Partially Mixed Estuary. Can. J. Fish. Aquat. Sci. 40:1543-1555.

Galbraith, P.S., Chassé, J., Shaw, J.-L., Dumas, J., Caverhill, C., Lefaivre, D. and Lafleur, C. 2020. Physical Oceanographic Conditions in the Gulf of St. Lawrence during 2019. DFO Can. Sci. Advis. Sec. Res. Doc. 2020/030. iv + 84 p.

Grégoire, F., Girard, L. and Boudreau, M. 2014. Résultats des relevés du programme de monitorage zonal atlantique (PMZA)-maquereau bleu (*Scomber scombrus* L.) réalisés dans le sud du golfe du Saint-Laurent en 2012 et 2013. Secr. can. de consult. sci. du MPO. Doc. de rech. 2014/075. v + 82 p.

Guisan, A. and Zimmermann, N. E. 2000. Predictive habitat distribution models in ecology. Ecol Modell, 135: 147–186.

Hurtubise, S. 1994. Pêche et caractéristiques biologiques du capelan (*Mallotus villosus*) dans le golfe du Saint-Laurent. Rapp. can. ind. sci. halieut. aquat. 94 /28: + 24 p.

Hurvich, C. M. and Tsai, C.-L. 1989. Regression and time series model selection in small samples,. Biometrika 76: 297–307.

Jacquaz, B., Able, K. W., and Leggett, W. C. 1977. Seasonal Distribution, Abundance, and Growth of Larval Capelin (*Mallotus villosus*) in the St. Lawrence Estuary and Northwestern Gulf of St. Lawrence. J. Fish. Res. Board. Can. 34: 2008-2014.

Le Cren, E. D. 1951. The length-weight relationship and seasonal cycle in gonad weight and condition in the Perch (*Perca flavescens*). J. Anim. Ecol. 20: 201–219.

Lehoux, C., Plourde S., and Lesage, V. 2020. Significance of dominant zooplankton species to the North Atlantic Right Whale potential foraging habitats in the Gulf of St. Lawrence: a bio-energetic approach. DFO Can. Sci. Advis. Sec. Res. Doc. 2020/033. iv + 44 p.

Lewis, K. P., Buren, A. D., Regular, P. M., Mowbray, F. K., and Murphy, H. M. 2019. Forecasting capelin *Mallotus villosus* biomass on the Newfoundland shelf. Mar. Ecol. Prog. Ser. 616: 171–183.

McQuinn I.H. 2009. Pelagic fish outburst or suprabenthic habitat occupation: legacy of the Atlantic cod (*Gadus morhua*) collapse in eastern Canada. Can. J. Fish. Aquat. Sci. 66: 2256–2262.

McQuinn, I. H., Plourde, S., St. Pierre, J. F., and Dion, M. 2015. Spatial and temporal variations in the abundance, distribution, and aggregation of krill (*Thysanoessa raschii* and *Meganyctiphanes norvegica*) in the lower estuary and Gulf of St. Lawrence. Prog. Oceanogr. 131: 159–176.

Ménard, N. 1998. Répartition spatiale et structure des bancs de poissons pélagiques dans une aire d'alimentation des cétacés de l'estuaire du Saint-Laurent. Thèse (M. Sc.)--Université Laval, 1998. Xi+ 123 pp

Mowbray, F.K. 2002. Changes in the vertical distribution of capelin (*Mallotus villosus*) off Newfoundland. ICES J. Mar. Sci. 59: 942-949.

Mullowney, D., Maillet, G., Dawe, E., Rose, G., and Rowe, S. 2016. Spawning delays of northern capelin (*Mallotus villosus*) and recovery dynamics: A mismatch with ice-mediated spring bloom? Prog. Oceanogr. 141: 144–152.

Murphy, H. M., Pepin, P., and Robert, D. 2018. Re-visiting the drivers of capelin recruitment in Newfoundland since 1991. Fish. Res. 200: 1–10.

O'Driscoll, R. L., Rose, G. A. and Anderson, J. T. 2002. Counting capelin: a comparison of acoustic density and trawl catchability. ICES J. Mar. Sci. 59: 1062-1071.

Ouellet, P., Bui, A. O. V., Lavoie, D., Chassé, J., Lambert, N., Ménard, N., and Sirois, P. 2013. Seasonal distribution, abundance, and growth of larval capelin (*Mallotus villosus*) and the role of the Lower Estuary (Gulf of St. Lawrence, Canada) as a nursery area. Can. J. Fish. Aquat. Sci. 70: 1508–1530.

Orlova, E. L., Dolgov, A. V., Rudneva, G. B., Oganin, I. A., and Konstantinova, L. L. 2009. Trophic relations of capelin Mallotus villosus and polar cod Boreogadus saida in the Barents Sea as a factor of impact on the ecosystem. Deep Sea Res. Part II Top. Stud. Oceanogr. 56: 2054-2067.

Orlova, E. L., Rudneva, G. B., Renaud, P. E., Eiane, K., Savinov, V., and Yurko, A. S. 2010. Climate impacts on feeding and condition of capelin *Mallotus villosus* in the Barents Sea: Evidence and mechanisms from a 30 year data set. Aquat. Biol. 10: 105–118.

Plourde, S., Joly, P., Runge, J. A., Zakardjian, B. and Dodson, J. J. 2001. Life cycle of *Calanus finmarchicus* in the lower St. Lawrence Estuary: the imprint of circulation and late timing of the spring phytoplankton bloom. Can. J. Fish. Aquat. Sci. 58: 647–658.

Plourde, S., Joly, P., Runge, J. A., Dodson, J. J. and Zakardjian, B. 2003. Life cycle of *Calanus hyperboreus* in the lower St. Lawrence Estuary and its relationship to local environmental conditions. Mar. Ecol. Prog. Ser. 255: 219–233.

Plourde, S., Lehoux, C., Johnson, C. L., Perrin, G., and Lesage, V. 2019. North Atlantic right whale (*Eubalaena glacialis*) and its food : ( I ) a spatial climatology of *Calanus* biomass and potential foraging habitats in Canadian waters. J. Plankton Res. 41: 667-685–19.

R Core Team. 2020. R: A language and environment for statistical computing. R Foundation for Statistical Computing, Vienna, Austria.

Vesin, J. P., Leggett, W. C., and Able, K. W. 1981. Feeding ecology of capelin (*Mallotus villosus*) in the estuary and western Gulf of St. Lawrence and its multispecies implications. Can. J. Fish. Aquat. Sci. 38: 257-267.

Wood, S.N. 2006. Low rank scale-invariant tensor product smooths for generalized additive mixed models. Biometrics. 62: 1025-1036.

Wood, S.N. 2017. Generalized Additive Models: An Introduction with R (2nd edition). Chapman and Hall/CRC.

Zuur, A. F., and Ieno, E. N. 2016. A protocol for conducting and presenting results of regression-type analyses. Methods Ecol. Evol.: 7: 636–645.

## TABLES

*Table 1. Summary of GAMs for the standardization of the larval index. The abundance of capelin larvae per m² is the response variable. The predictors included a spatial effect where x.m and y.m are projected coordinates (in meters/$10^5$) in the lambert conic conformal projection, the sampling (S) date, the hatching date (H) and the number of days since hatch (S date – H date). The negative binomial distribution uses a log link between abundance and predictors. Ti is a tensor product interaction and te is a full tensor product smooth used when main effects are not included. The selected model with the lowest AIC is in bold. The ∆AIC is the difference between the AIC of each model and the model in bold. Df: is the number of degrees of freedom. Weight is the Akaike weight.*

| Models | AIC | ∆AIC | df | Weight | % deviance explained |
|---|---|---|---|---|---|
| Log($Nm^{-2}$)~ ti(S date) + ti(H date) + ti(S date, H date) | 5413 | 1371 | 10.2 | 0 | 7.9 |
| Log($Nm^{-2}$)~ te(x.m × y.m × year) | 4100 | 57.9 | 259.7 | 0 | 85.7 |
| Log($Nm^{-2}$)~ te(x.m × y.m × year) + s(S date) | 4061 | 19.2 | 258.9 | 0 | 86.3 |
| Log($Nm^{-2}$)~ te(x.m × y.m × year) + s(S date) +s(H date) | 4056 | 14.4 | 258.9 | 0.001 | 86.6 |
| **Log($Nm^{-2}$)~ te(x.m × y.m × year) + ti(S date) + ti(H date) + ti(S date, H date)** | **4042** | **0.0** | **268.3** | **0.801** | **87.0** |
| Log($Nm^{-2}$)~ te(x.m × y.m × year) + ti(S date) + ti(Days since hatch) + ti(S date, Days since hatch) | 4045 | 2.8 | 267 | 0.199 | 86.9 |

*Table 2. Data used in the capelin abundance models and anticipated effects on capelin Kn and survival.*

| Period | | Variable | Units | Interpretation/role in capelin abundance model | Reference |
|---|---|---|---|---|---|
| nGSL | sGSL | | | | |
| 1990-2020 | | nGSL and sGSL bottom-trawl surveys abundance indices (August-September) | mean number per tow | Proxy of capelin population abundance in nGSL (2-3 years old) and sGSL (1-2 years old) | Chamberland et al. (2022b) |
| - | 1983-2019 | Larval abundance index (sGSL, June) | mean N $m^{-2}$ | Proxy of capelin population reproductive output | - |
| 1984-2020 | 1986-2020[1] | Kn June (Spring, mostly 3-4 years old) | - | Greater Kn indicative of higher capelin survival after winter | - |
| 1999-2020 | 1990-2020 | Kn August-September (Fall) (mostly 1-2 years old) | - | Greater Kn indicative of higher capelin survival potential during next winter | - |
| 1980-2019 | 1990-2019[2] | SST June and SST May-August | °C | Higher SST favors capelin Kn in Fall and survival potential during next winter | Galbraith et al. 2020 |
| 1980-2019 | 1990-2019 | Spring timing | week of the year SST reaches 10C | Earlier warming favors zooplankton production, capelin Kn and survival after winter (t0) | |
| 1980-2019 | 1990-2019 | Timing of ice retreat | julian day | Earlier ice retreat favors an earlier timing of the spring bloom and zooplankton production, and capelin survival | |
| 1998-2018 | | Bloom timing | Julian day | Earlier timing of the spring bloom favors earlier zooplankton production, and capelin survival | Blais et al. 2019 |
| 2001-2018 | | *C. fin.* abundance (June) | $10^3$ ind $m^{-2}$ | Favors capelin Kn (June) (and spring survival) | |
| | | *C. hyp*. Abundance (June) | $10^3$ ind $m^{-2}$ | | |
| | | *Pseudocalanus* spp abundance (June) (only in nwGSL) | $10^3$ ind $m^{-2}$ | Favors capelin larvae survival | |
| | | *C. fin*. development index (June) | C1-C4/C1-C6 | Indices of the population development state: the higher the index, the later is the development of *C.fin.* and the lesser is Kn (June) (and spring survival) | |

| Period | | Variable | Units | Interpretation/role in capelin abundance model | Reference |
|---|---|---|---|---|---|
| nGSL | sGSL | | | | |
| 2001-2019 | | *C. hyp*. development index (June) | C4/C1-C4 | Indices of the population development state: the higher the index, the earlier is the development of *C. hyp*. and the higher is capelin Kn (June) and survival (June) | Blais. M. DFO, personnal communication |
| 1992-2019 | | *C. fin abundance Jul-Sep* | ind $m^{-2}$ | Favors capelin Kn (August-September) (and next winter survival) | Blais et al. 2019 |
| | | *C. hyp abundance Jul-Sep* | ind $m^{-2}$ | | |
| | | *Pseudocalanus abundance (Jul-November) (sGSL and neGSL)* | ind $m^{-2}$ | Favors capelin larvae survival | |

[1] high proportion of missing years in the time series

[2] the physical environmental variables can be accessed before 1990 but was not extracted because it was not necessary for this time series

*Table 3. Summary of selected GAMs for capelin Kn and abundance at age 2 (M2) and at age 3 (M3) in the neGSL. Other models considered are presented in Appendix 4 Tables A.4.1, A.4.4 and A.4.5. The effect of each selected predictor on the response variable can be positive (+), negative (-), bell-shaped (∩) or U-shaped (∪). Non-significant effects are noted with n.s. The performance of each model is evaluated with the R², the comparison of deviance explained with bootstrap (* for significantly higher than the distribution obtained by bootstrap and n.s. otherwise) and the Pearson's correlation between predicted and observed values during the Jackknife procedure.*

| Response variable | Years | Variables | Effect | $R^2$ | % deviance explained | Bootstrap | Jacknife |
|---|---|---|---|---|---|---|---|
| Kn June | 1984-2019 | SST June<br>Timing of ice retreat | -n.s.<br>- | 0.18 | 23 | n.s. | 0.16 |
| Abundance (M2) | 1995-2020 | Kn June<br>Timing of ice retreat t-1 | +.<br>-n.s. | 0.37 | 44 | * | 0.55 |
| Abundance (M3) | 1997-2020 | Kn June t-1<br>Timing of ice retreat t-2 | +<br>∩ | 0.40 | 49 | * | 0.47 |

*Table 4. Summary of selected GAMs for capelin Kn and abundance at age 2 (M2) and at age 3 (M3) in the nwGSL. Other models considered are presented in Appendix 4 Table A.4.2, A.4.6 and A.4.7. The effect of each selected predictor on the response variable can be positive (+), negative (-), bell-shaped (∩) or U-shaped (∪). Non-significant effects are noted with n.s. The performance of each model is evaluated with the R², the comparison of deviance explained with bootstrap (* for significantly higher than the distribution obtained by bootstrap and n.s. otherwise) and the Pearson's correlation between predicted and observed values during the Jackknife procedure.*

| Response variable | Years | Variables | Effect | $R^2$ | % deviance explained | Bootstrap | Jacknife |
|---|---|---|---|---|---|---|---|
| Kn June | - | No models selected | - | - | - | - | - |
| Kn August (nGSL) | 2001-2018 | *C. finmarchicus* dev. index (early summer) | - | 0.50 | 55 | * | 0.56 |
| Abundance (M2) | 1993-2019 | *C. finmarchicus* abundance Jul-Sep t-1<br>Timing of ice retreat | +<br>-n.s. | 0.25 | 33 | * | 0.44 |
| Abundance (M3) | 1992-2020 | Kn June t-1 | ∩ | 0.46 | 51 | * | 0.49 |

*Table 5. Summary of selected GAMs for capelin Kn and abundance at age 1(M1) and at age 2 (M2) in the sGSL. Other models considered are presented in Appendix 4 Table A.4.3, A.4.8 and A.4.9. The effect of each selected predictor on the response variable can be positive (+), negative (-), bell-shaped (∩) or U-shaped (∪). Non-significant effects are noted with n.s. The performance of each model is evaluated with the $R^2$, the comparison of deviance explained with bootstrap (* for significantly higher than the distribution obtained by bootstrap and n.s. otherwise) and the Pearson's correlation between predicted and observed values during the Jackknife procedure.*

| Response variable | Years | Variables | Effect | $R^2$ | % deviance explained | Bootstrap | Jacknife |
|---|---|---|---|---|---|---|---|
| Kn June | 2006-2018 | *C. hyperboreus* dev. index (early summer) | + | 0.78 | 83 | * | 0.84 |
| Kn September | 1990-2019 | SST May- August | - | 0.22 | 27 | * | 0.34 |
| Kn September | 1999-2019 | *C.finmarchicus abundance Jul-Sep* | + | 0.50 | 54 | * | 0.48 |
| Abundance (M1) | 1990-2019 | Timing of ice retreat | - | 0.31 | 34 | * | 0.47 |
| Abundance (M2) | 1991-2019 | SST May-August t-1<br>Timing of ice retreat | +<br>- | 0.57 | 61 | * | 0.67 |

# FIGURES

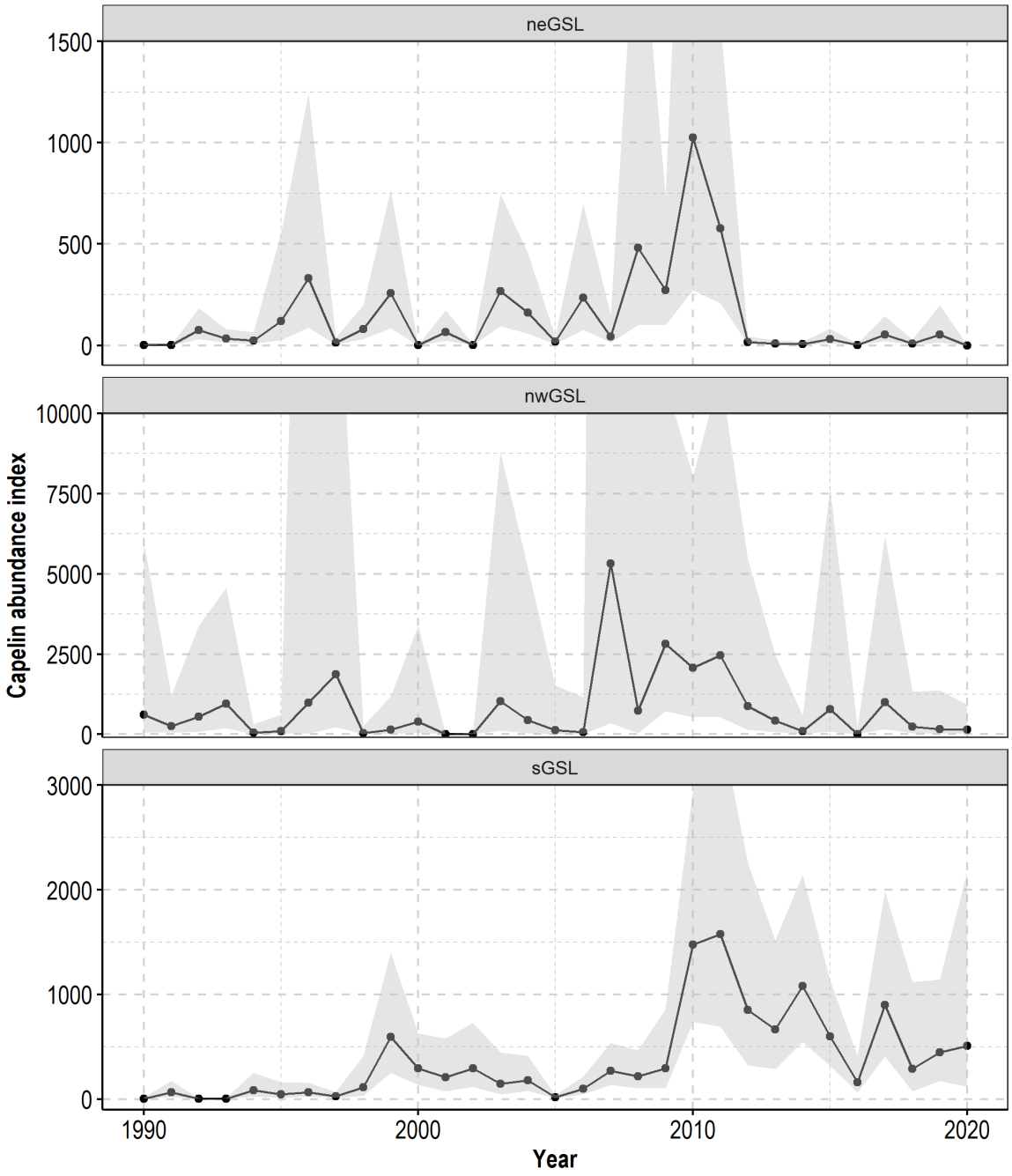


*Figure 1. Capelin abundance indices calculated using the multidisciplinary trawl surveys in August in the neGSL and nwGSL and September in the sGSL. Shaded area represent the confidence intervals around the estimated indices. See figure 2 for region locations.*

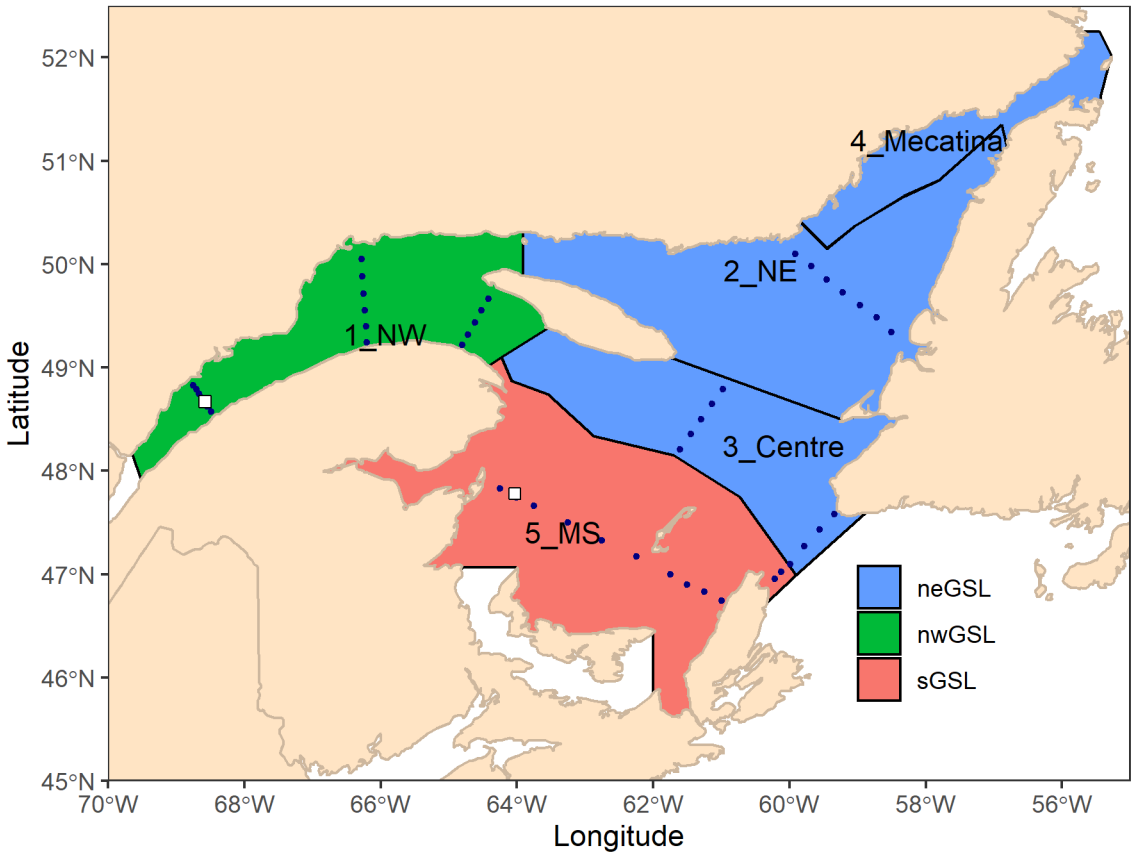


*Figure 2. Regions of the ecosystem approach used to extract environmental data. Colors correspond to the regions corresponding to the different capelin abundance indices, labels and black lines give the corresponding ecosystem approach regions, white squares: position of AZMP fixed stations for zooplankton samples (Jul-Sep or Jul-Nov), black circles: position of AZMP transects sampled in early summer.*

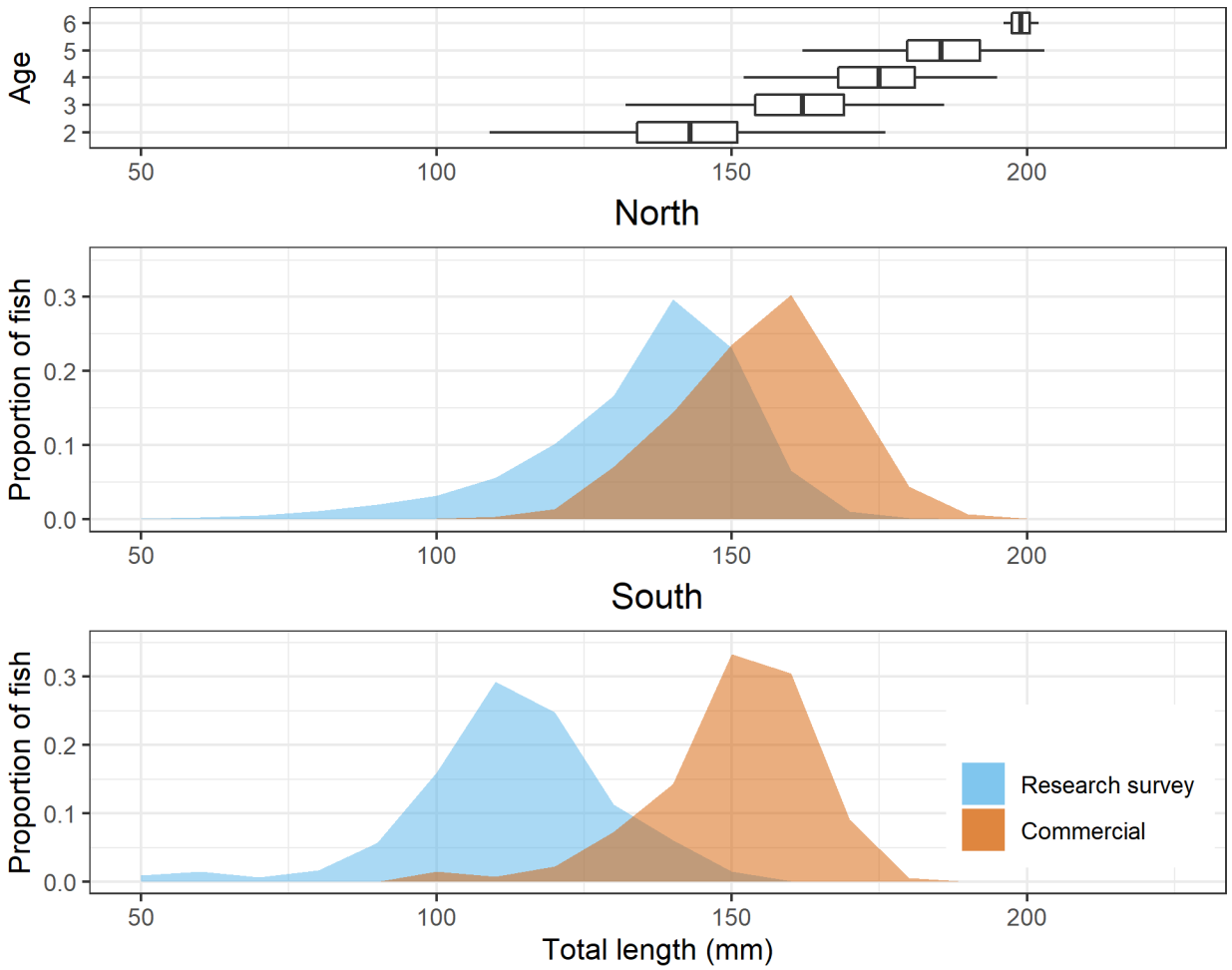


*Figure 3. Length at age (first row, 1984-1993 GSL capelin data, Hurtubise 1994) and length distribution for nGSL and sGSL RV surveys (blue) compared to length distribution in the commercial fishery (orange). For the commercial length distributions, NAFO Divisions 4R and 4S were plotted in the North panel, whereas 4T commercial data was plotted in the South panel.*

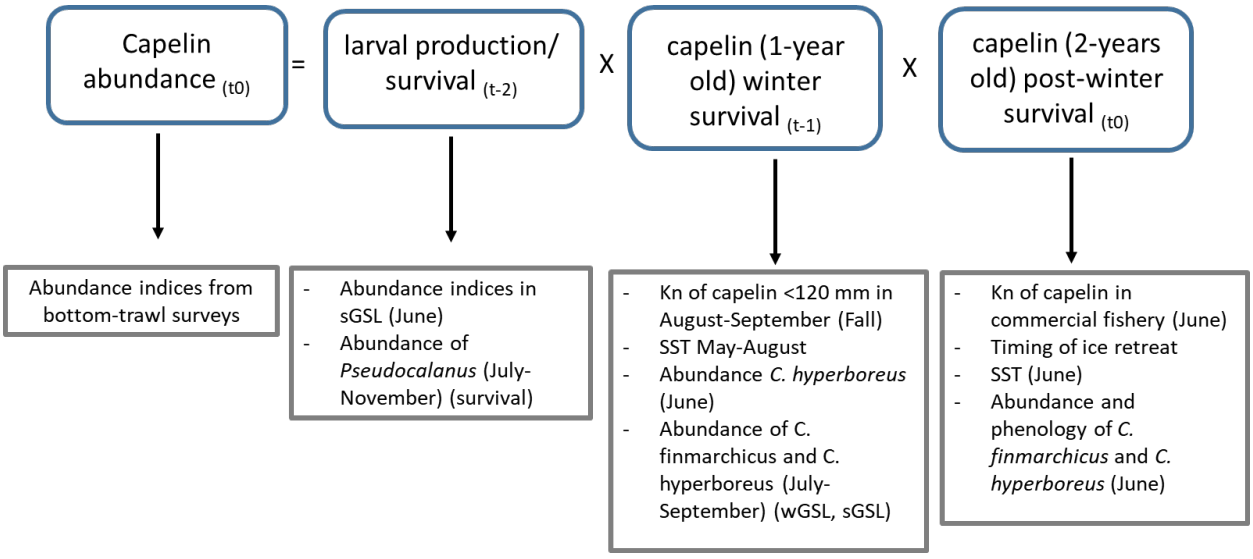


*Figure 4. Capelin abundance model M2 structure and associated variables. Kn or its environmental predictors identified in GAMs are used as a proxy of capelin survival potential during winter or in spring. See Table 2 for a description of the expected effects of environmental proxies on capelin Kn and survival.*

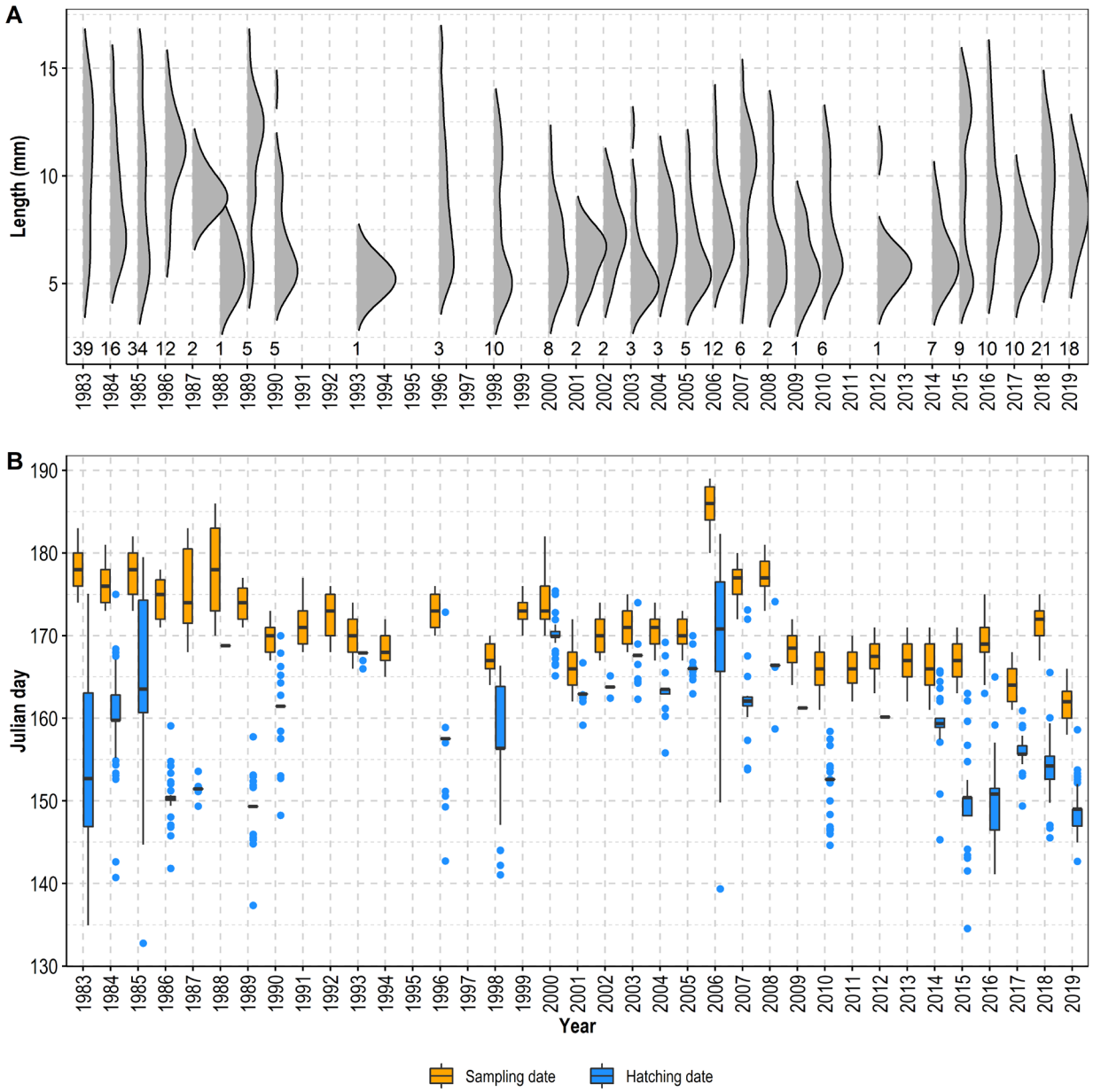


*Figure 5. Capelin larvae length distribution (A). Number of stations where larvae lengths were sampled are indicated above the x-axis. Sampling date (orange) and calculated hatching date (blue) for the larval survey in the sGSL (B).*

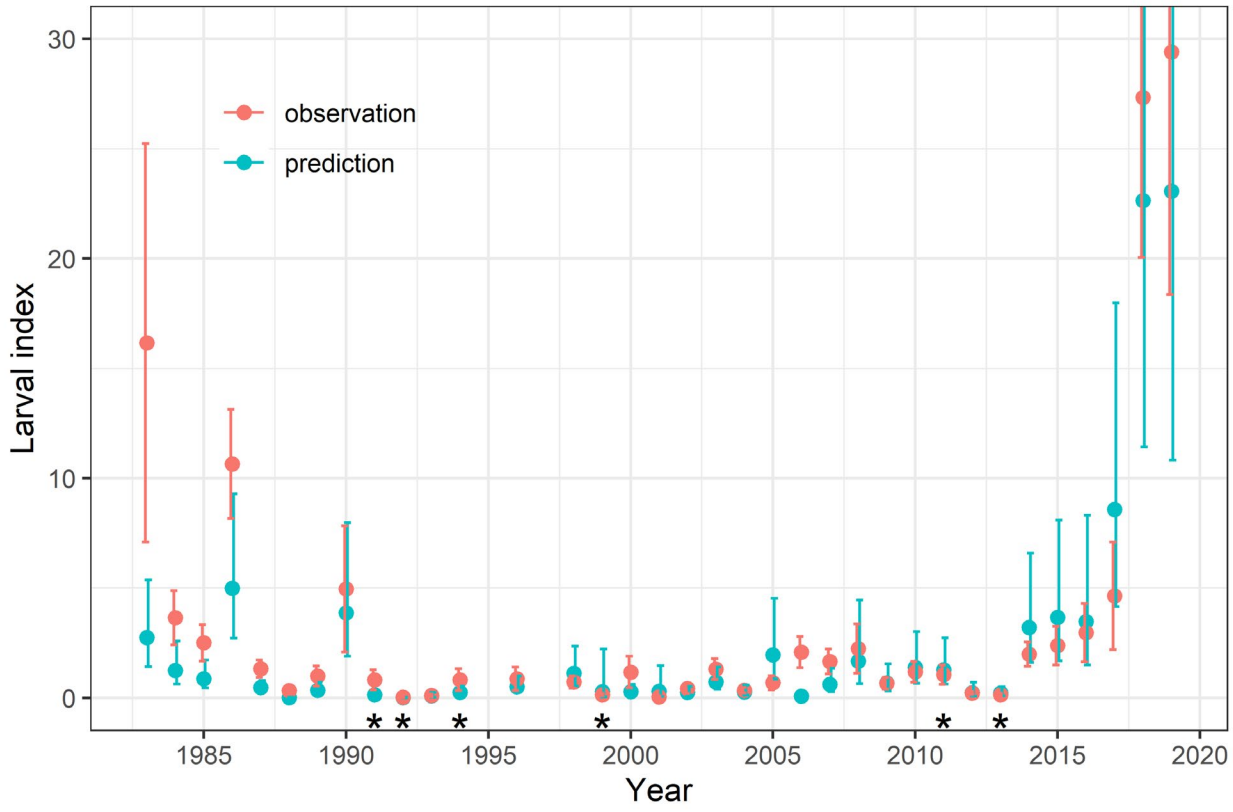


*Figure 6. Observed larval index (orange) with standard error and standardized larval index (blue) with mean model standard error. *: Years with no larvae measurements for which the 1983-2019 mean hatching date was used.*

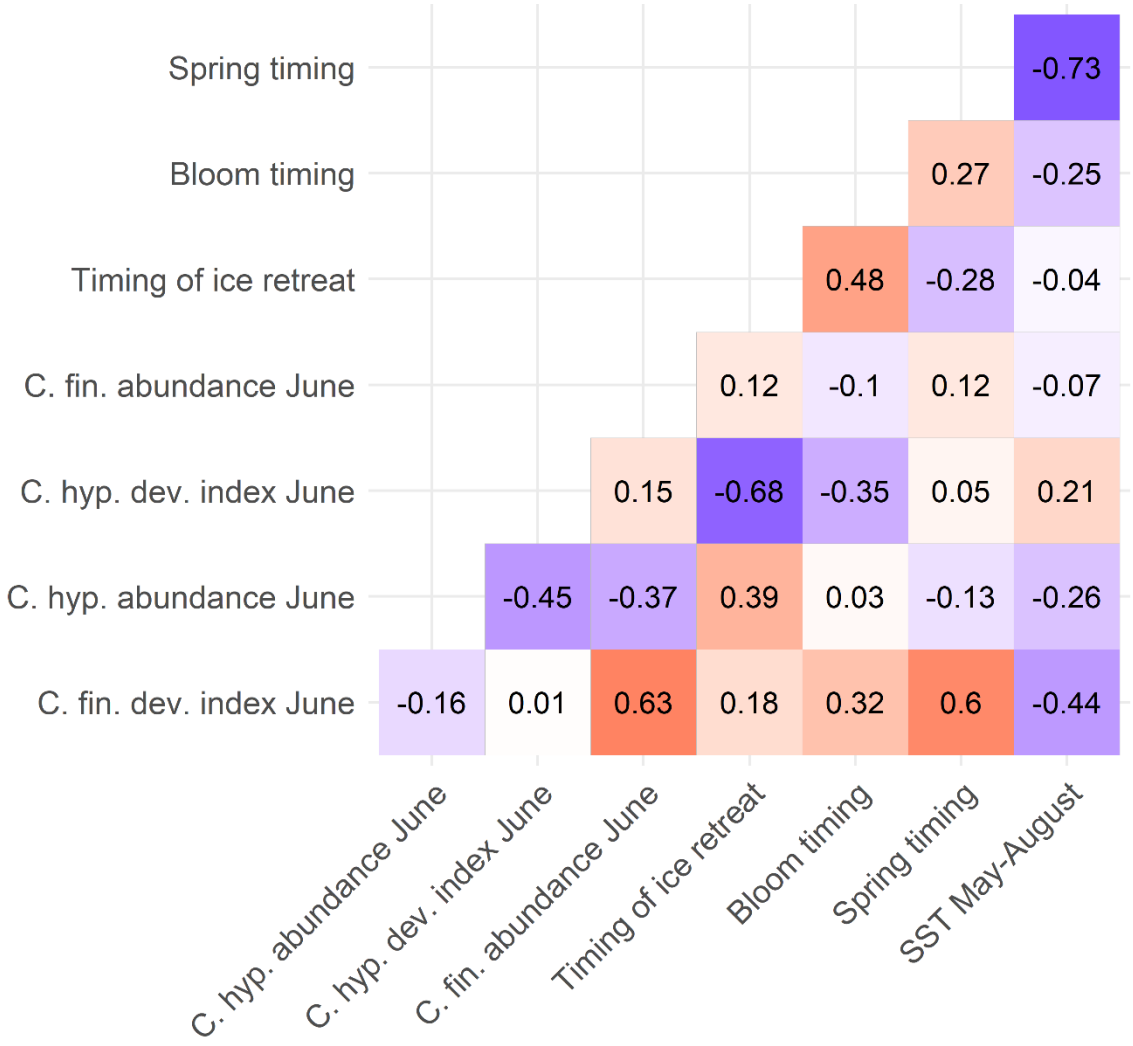


*Figure 7. Pearson's correlation coefficient between zooplankton and physical environment indices in the neGSL. Blue for negative correlation and red for positive correlation.*

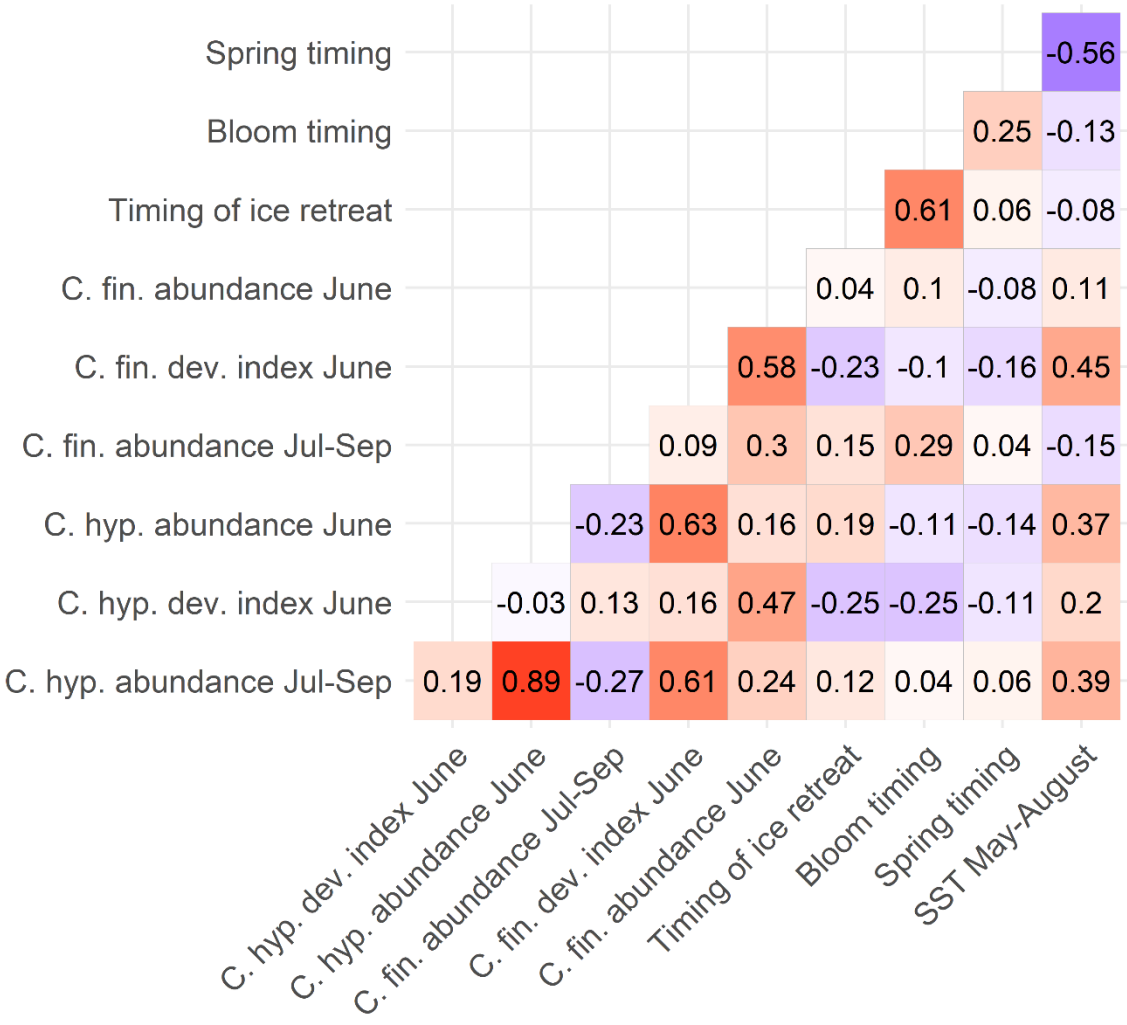


*Figure 8. Pearson's correlation coefficient between zooplankton and physical environment indices in the nwGSL. Blue for negative correlation and red for positive correlation.*

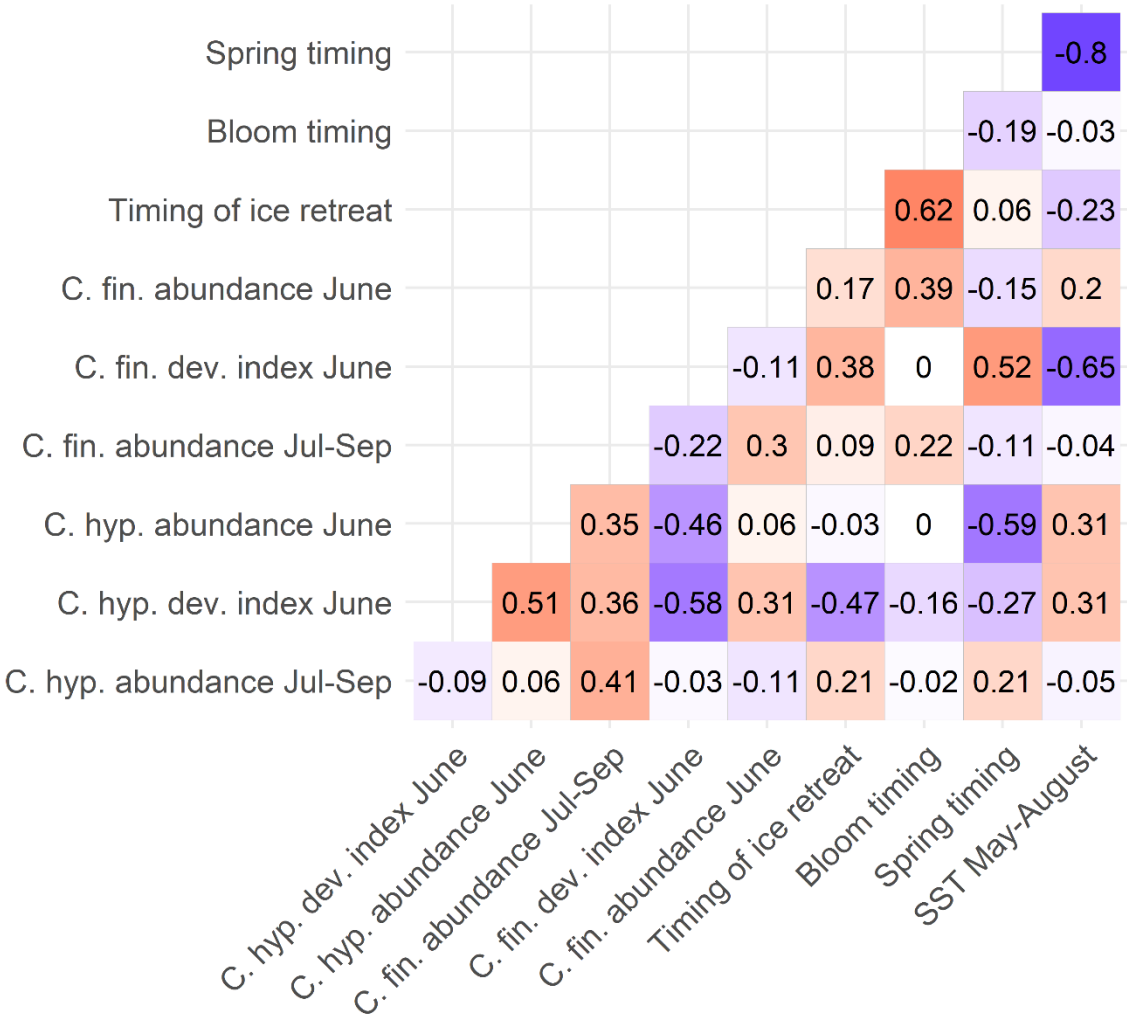


*Figure 9.Pearson's correlation coefficient between zooplankton and physical environment indices in the sGSL. Blue for negative correlation and red for positive correlation.*

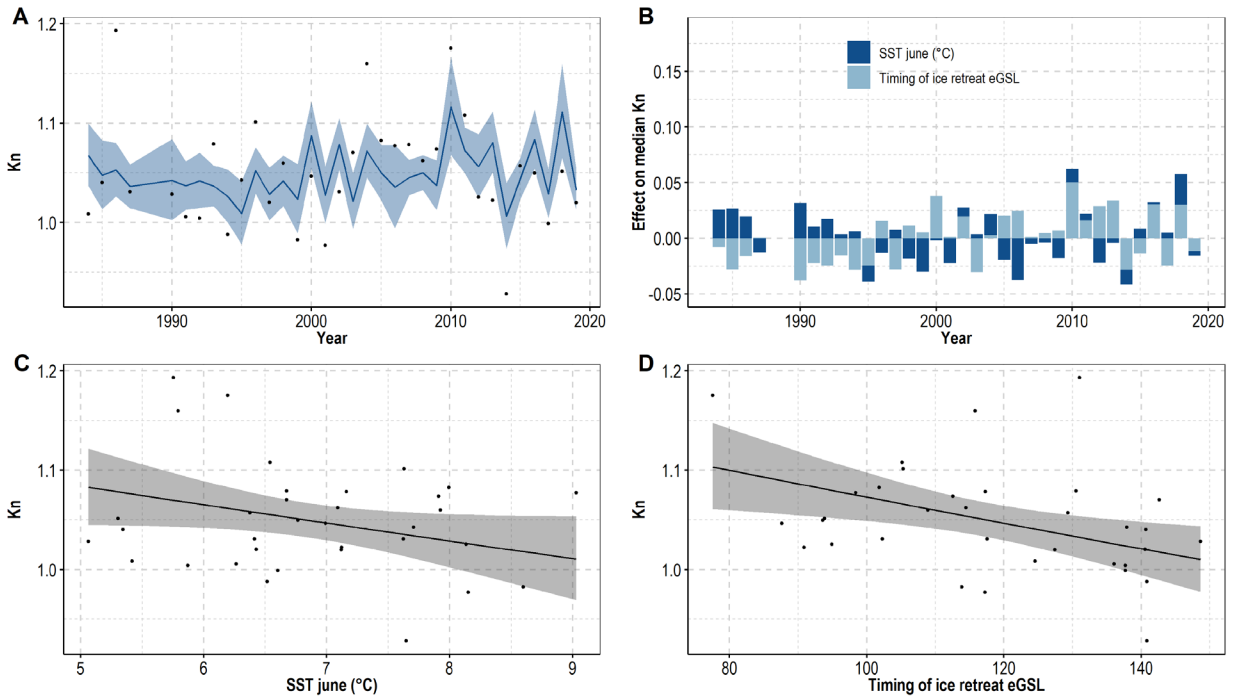


*Figure 10. Selected GAM for Kn in June in the neGSL: A) Observed Kn (black circles) are plotted against GAM predictions (blue line) and the 95% confidence intervals on the predictions (shaded blue area), B) Contribution of each variable to the predicted Kn every year, C) Effect of sea surface temperature in June, and D) timing of ice retreat (Julian day) on Kn. Grey areas: 95% confidence intervals.*

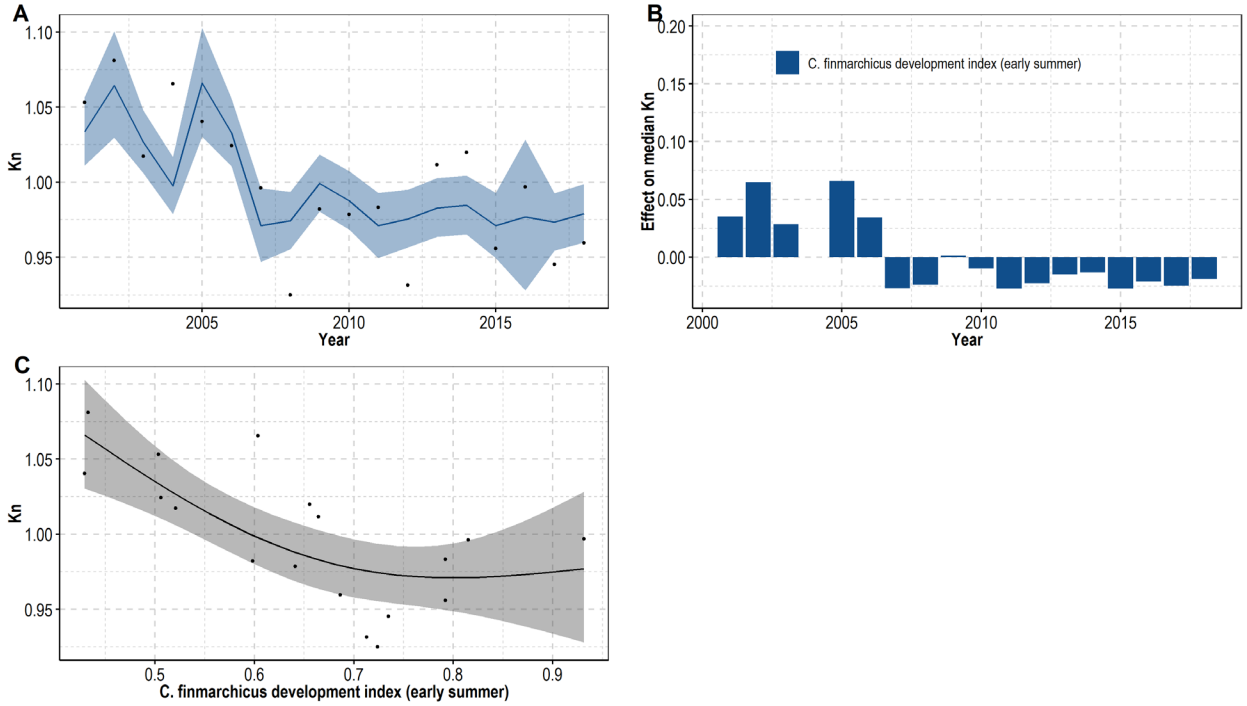


*Figure 11. Selected GAM for Kn in August in the nGSL: A). Observed Kn (black circles) are plotted against GAM predictions (blue line) and the 95% confidence intervals on the predictions (shaded blue area), B). Contribution of each variable to the predicted Kn every year, C) Effect of C. finmarchicus development index on Kn. Grey areas: 95% confidence intervals.*

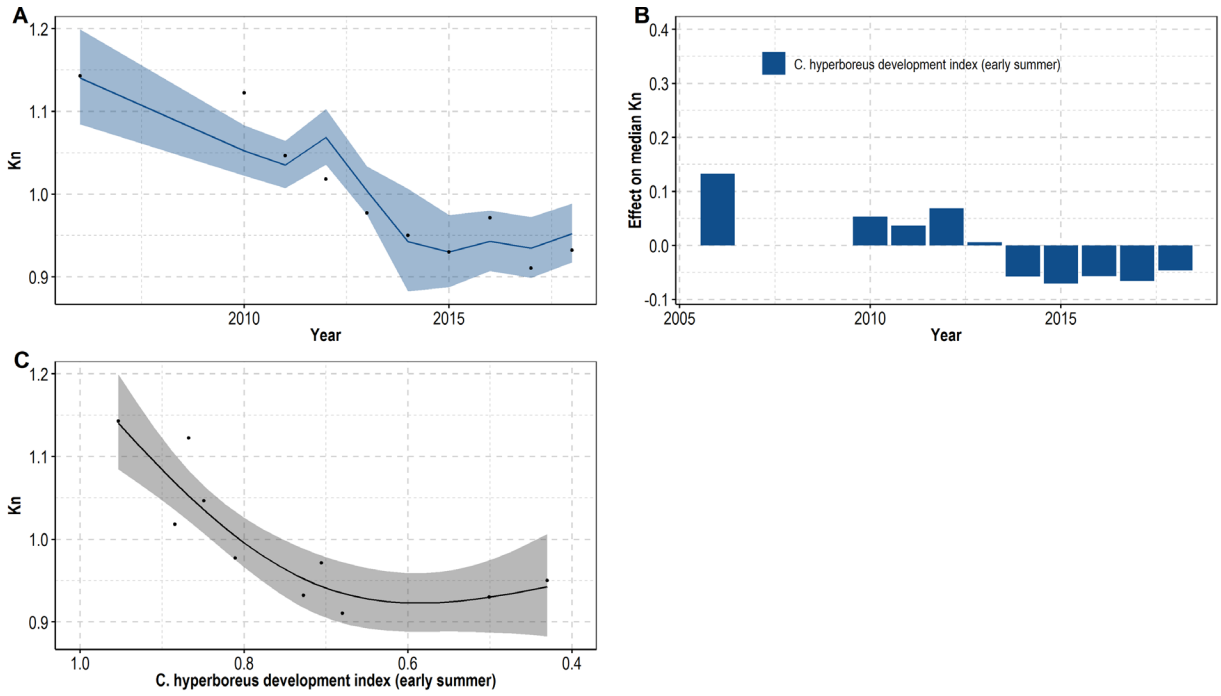


*Figure 12. Selected GAM for Kn in June in the sGSL: A) Observed Kn (black circles) are plotted against GAM predictions (blue line) and the 95% confidence intervals on the predictions (shaded blue area), B) Contribution of each variable to the predicted Kn every year, C) Effect of C. hyperboreus development index (proportion of CIV) on Kn. Grey areas: 95% confidence intervals.*

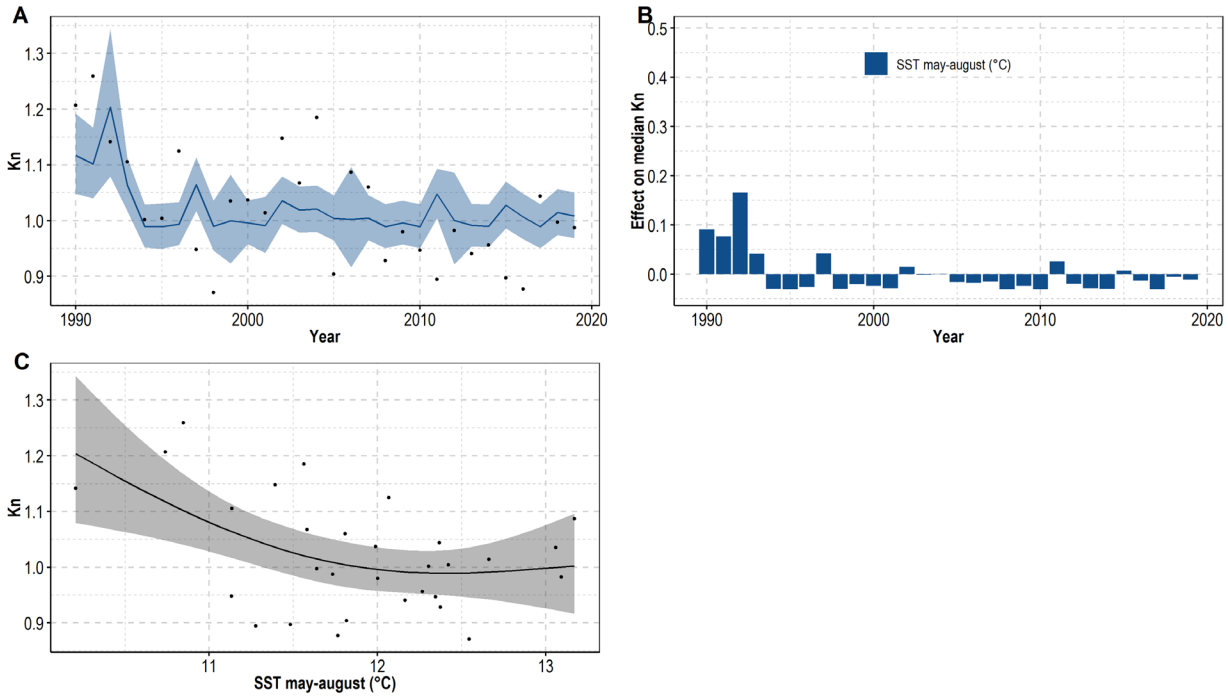


*Figure 13. Selected GAM for Kn in September in the sGSL: A) Observed Kn (black circles) are plotted against GAM predictions (blue line) and the 95% confidence intervals on the predictions (shaded blue area), B) Contribution of each variable to the predicted Kn every year, C) Effect of sea surface temperature in May-August on Kn. Grey areas: 95% confidence intervals.*

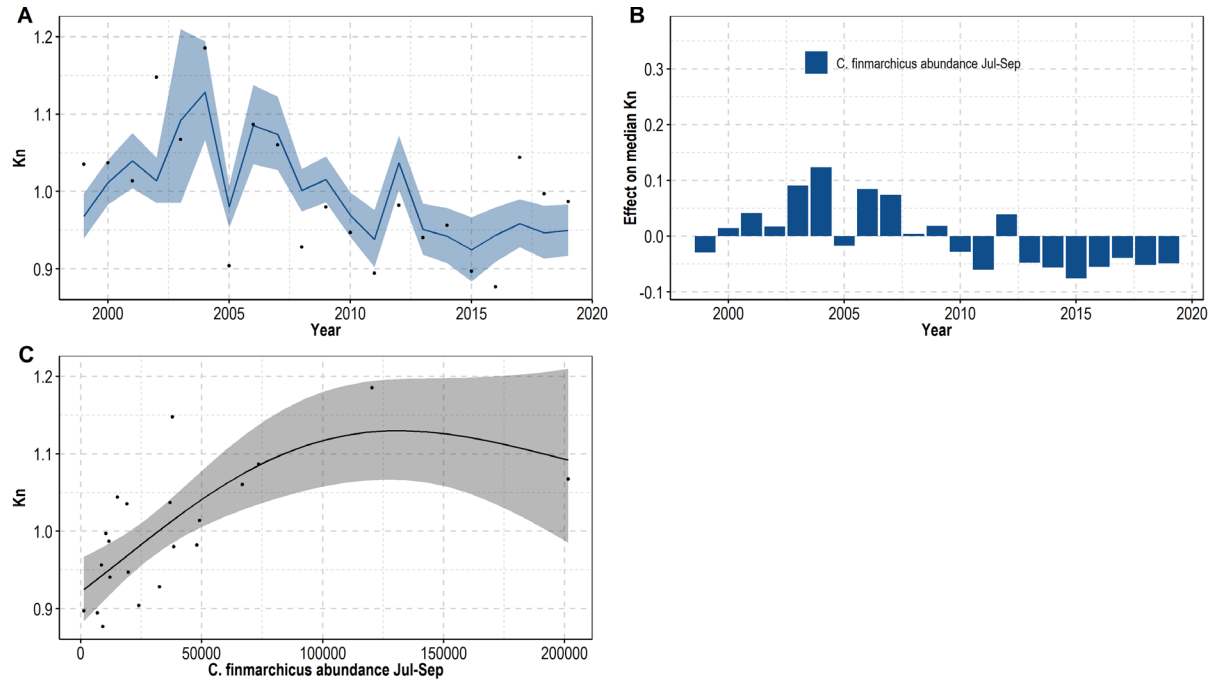


*Figure 14. Selected GAM for Kn in September in the sGSL: A) Observed Kn (black circles) are plotted against GAM predictions (blue line) and the 95% confidence intervals on the predictions (shaded blue area), B) Contribution of each variable to thEe predicted Kn every year, C) Effect of C. finmarchicus abundance in July-September (ind $m^{-2}$) on Kn. Grey areas: 95% confidence intervals.*

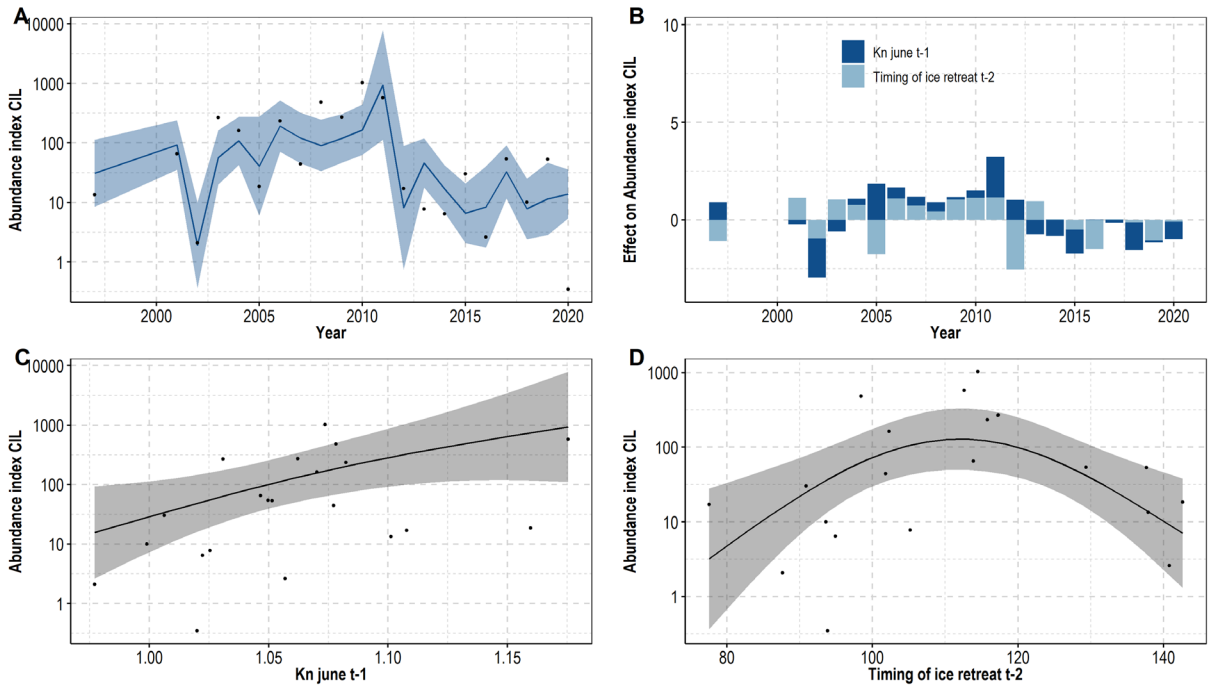


*Figure 15. Selected GAM for capelin abundance index at age 3 in the neGSL (M3): A) Capelin abundance index (black circles) are plotted against GAM predictions (blue line) and the 95% confidence intervals on the predictions (shaded blue area), B) Contribution of each variable to the predicted abundance index every year, C) Effect of Kn in June at age 2 and D) the timing of ice retreat at age 1 on capelin abundance index. Grey areas: 95% confidence intervals.*

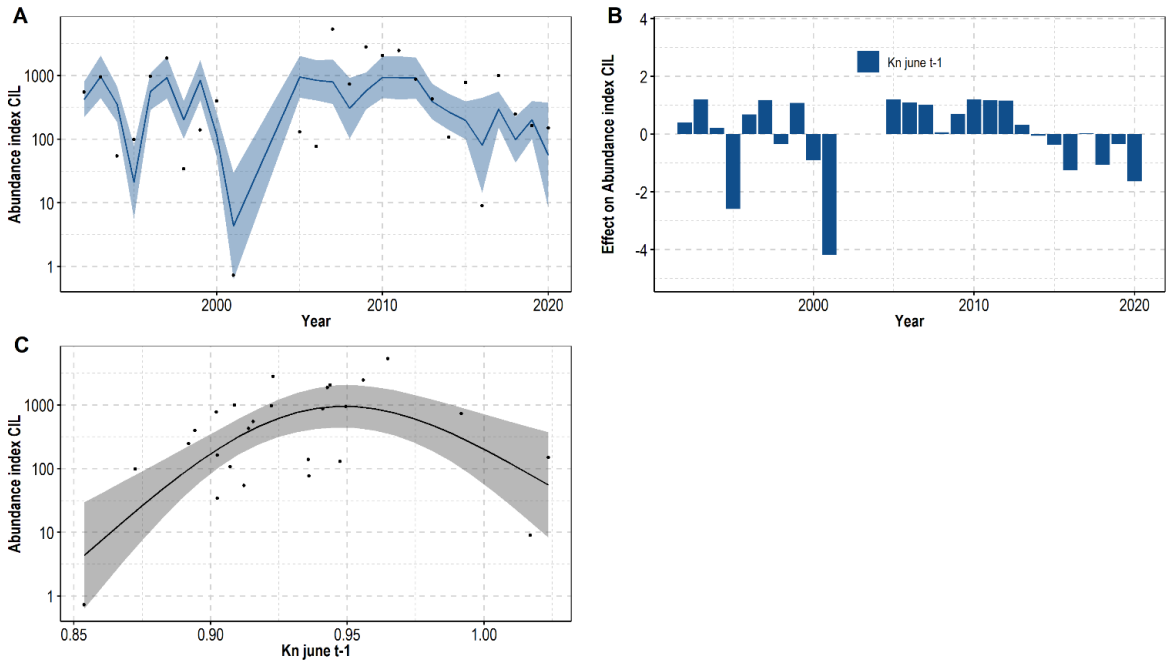


*Figure 16. Selected GAM for capelin abundance index at age 3 in the nwGSL (M3): A) Capelin abundance index (black circles) are plotted against GAM predictions (blue line) and the 95% confidence intervals on the predictions (shaded blue area), B) Contribution of each variable to the predicted abundance index every year, C) Effect of Kn in June at age 2 on capelin abundance index. Grey areas: 95% confidence intervals.*

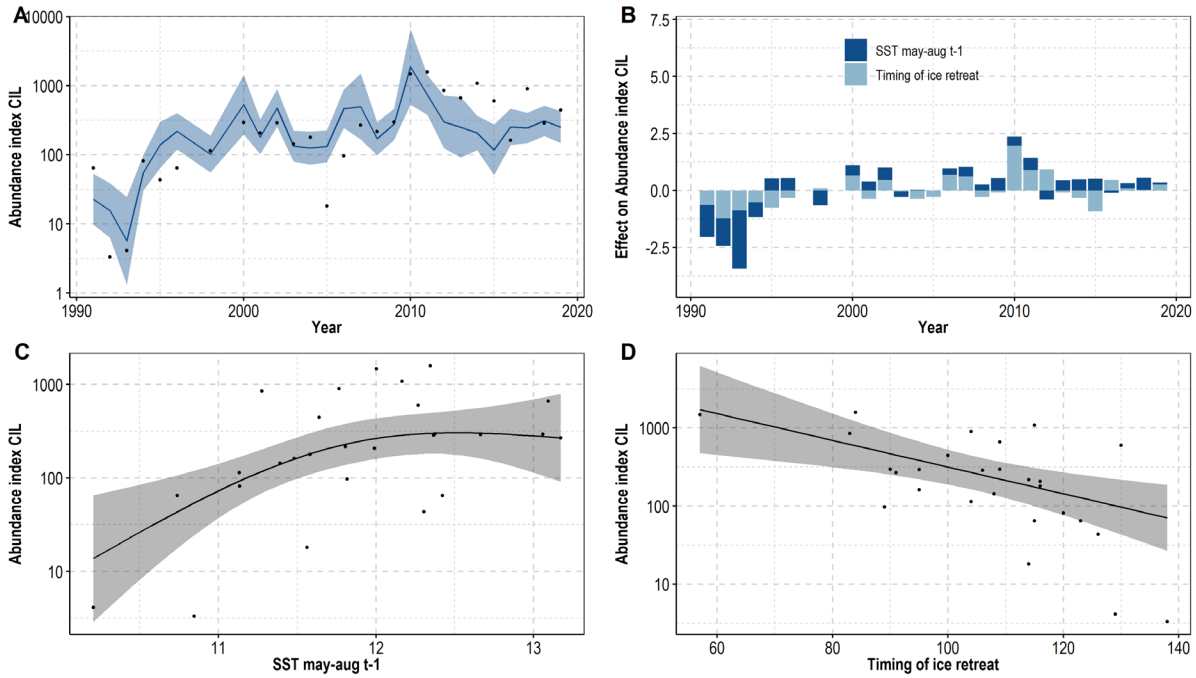


*Figure 17. Selected GAM for capelin abundance index at age 2 in the sGSL (M2): A) Capelin abundance index (black circles) are plotted against GAM predictions (blue line) and the 95% confidence intervals on the predictions (shaded blue area), B) Contribution of each variable to the predicted abundance index every year, C) Effect of SST in May-August at age 1 and D) timing of ice retreat at age 2 on capelin abundance index. Grey areas: 95% confidence intervals..*

# APPENDIX 1


*Figure A.1.1. Methods (y-axis) to calculate hatching date for each station and each year. Stations with 0 abundance were omitted on this figure for increased interpretability. Stations were grouped (color-coded) according to their abundance of larvae.*

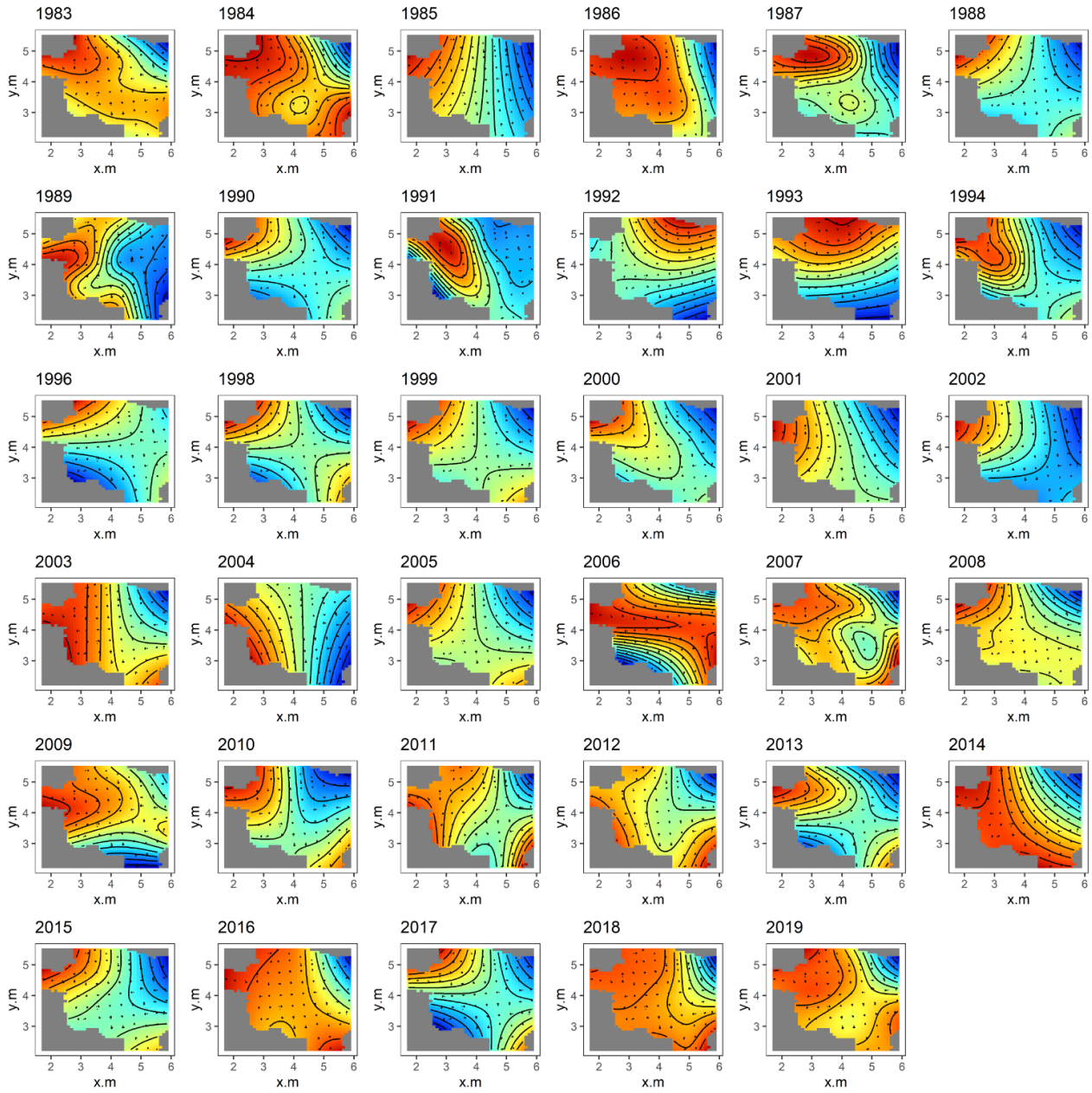


*Figure A.1.2. Spatial effect on larval abundance for the selected GAM used to calculate the larval index. Effects are presented in the scale of the linear predictor with blue to red representing negative to positive effect on larval abundance. Black points: position of stations, black line: contour lines. Other effects for this GAMs are presented in figure A.1.3. Equation of selected GAM:Log(Nm-2)~ te(x.m × y.m × year) + ti(S date) + ti(H date) + ti(S date, H date)*

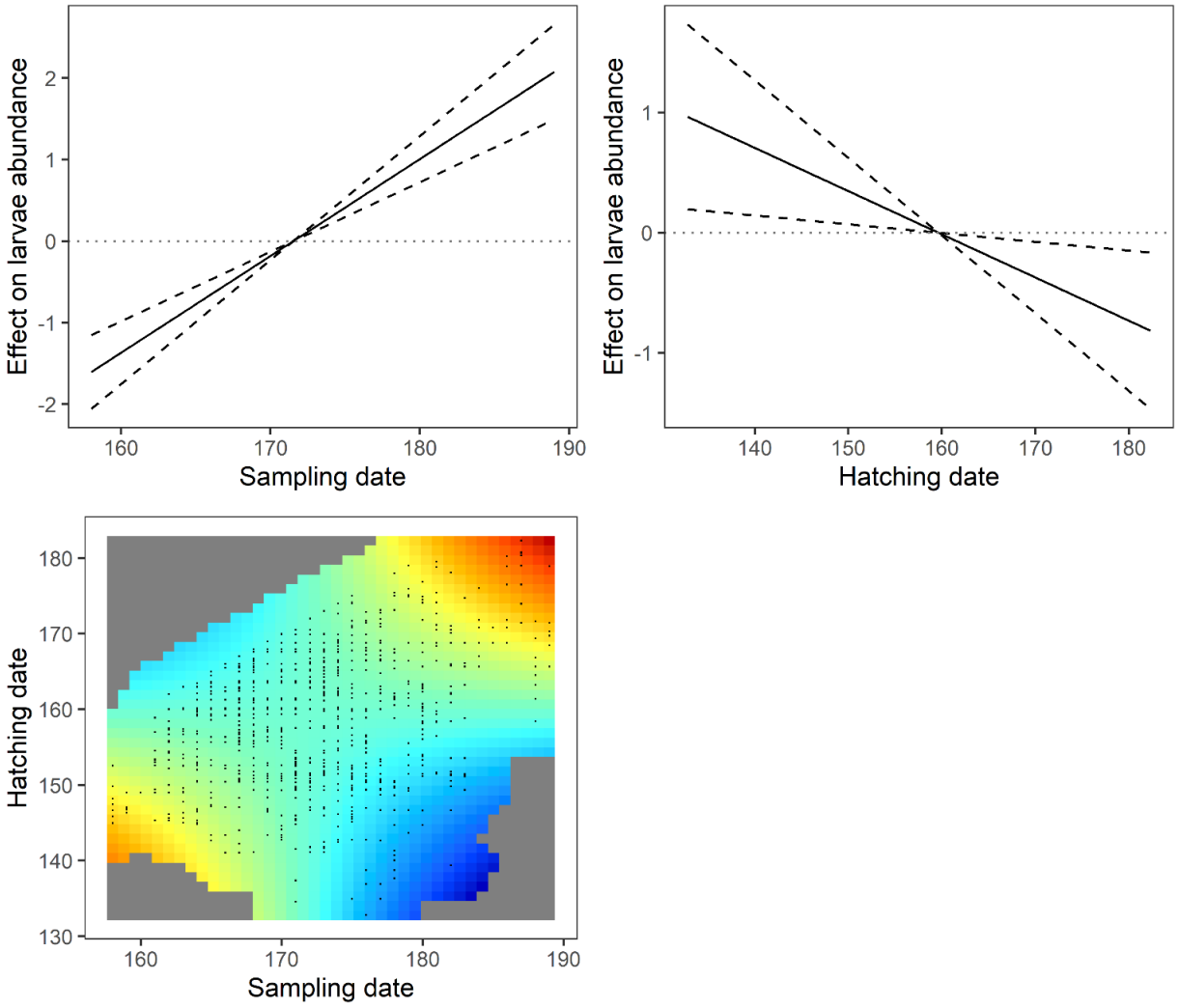


*Figure A.1.3. Effect of sampling and hatching date (top pannels) and their tensor product interaction (bottom) on larval abundance. Solid line: main effect; dashed line: 95$^{th}$ confidence intervals; grey dotted line: intercept. Dots in the interaction panel represent data. Negative-Positive effect of abundance=Blue-Red. Other effects for this GAMs are presented in figure A.1.2. Equation of selected GAM:Log(Nm-2)~ te(x.m × y.m × year) + ti(S date) + ti(H date) + ti(S date, H date).*

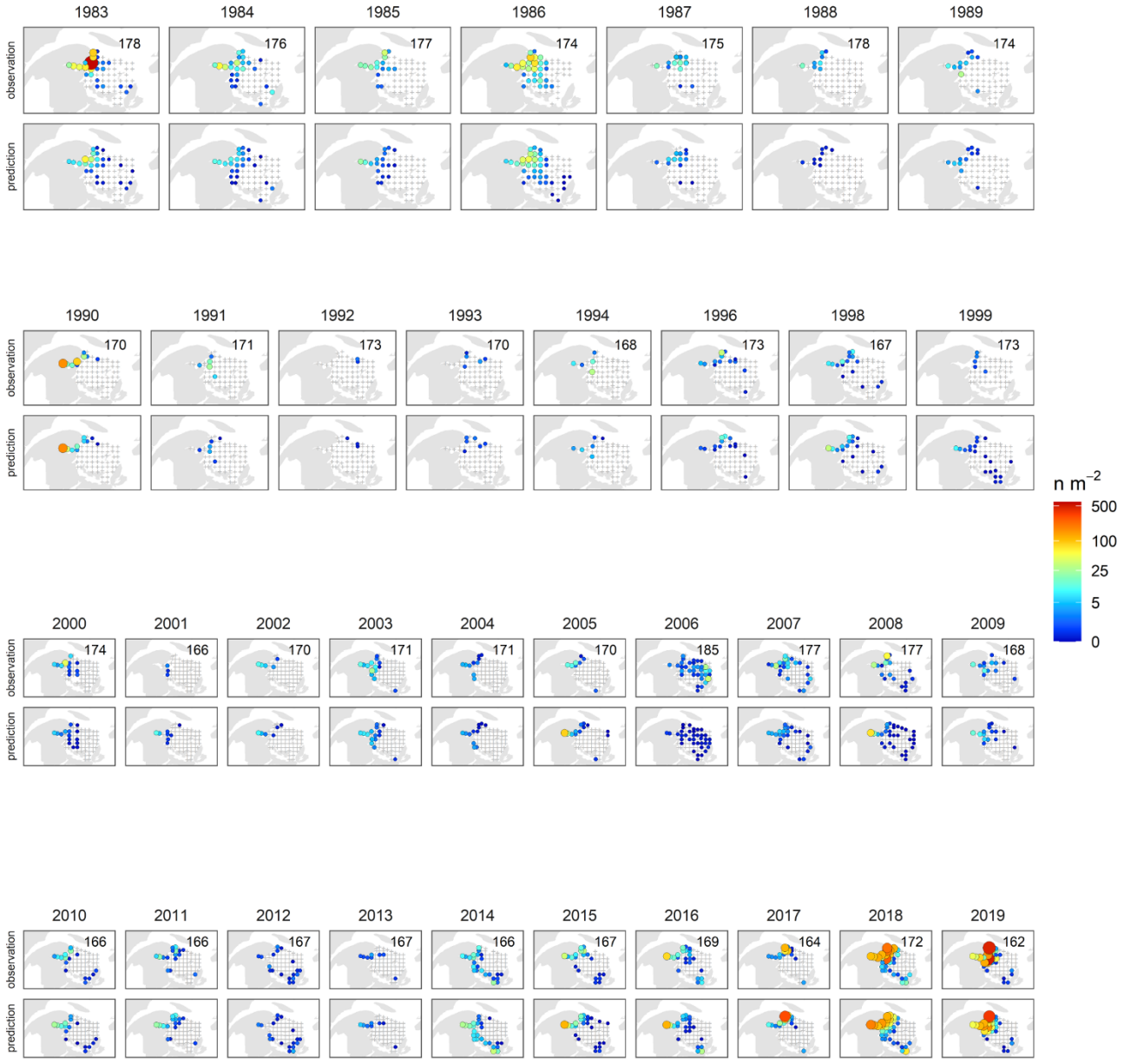


*Figure A.1.4. Sampled larval abundance (upper 'observation' panels) and GAM-standardize abundance (lower 'prediction' panels) at each year. Grey crosses represent absence of larvae. Color and size of the bubbles change with log-transform larval abundance. Mean sampling date for each year is shown in the upper-right of each map of the 'observation' panels.*

## APPENDIX 2

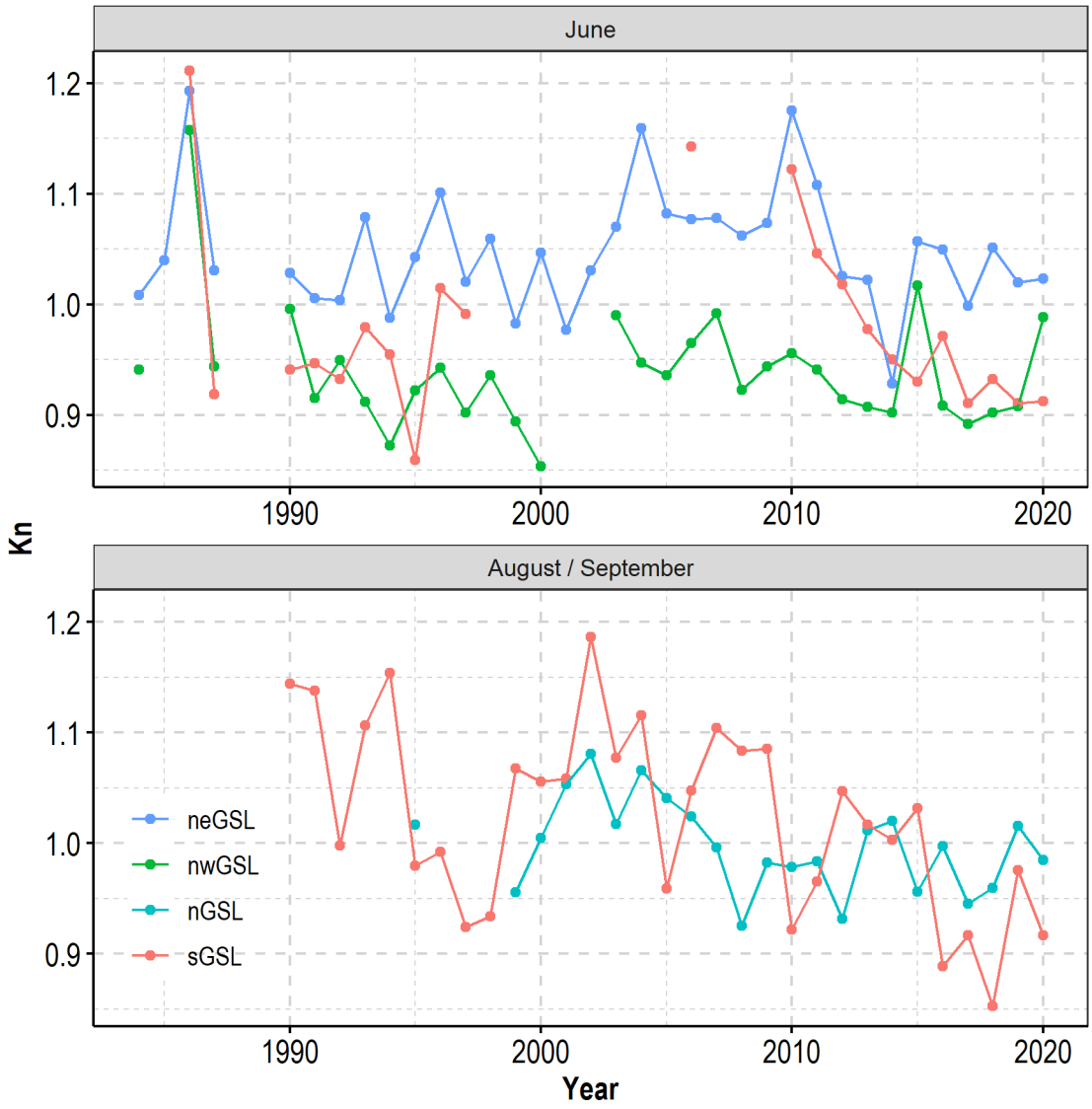


*Figure A.2.1. Temporal variation of the standardized Kn for June (commercial catches) and for fish smaller than 120 mm in August (nGSL) and September (sGSL). Note that data are not lagged.*


*Figure A.2.2. Temporal variation of environmental data extracted from the ecosystem approach matrix and used in the Kn and capelin abundance models. Note that the time series are not lagged in this figure. Timing of ice retreat is expressed in Julian day, spring timing in week of year, SST °C, abundance of copepods in June $10^3$ ind $m^{-2}$ (ind $m^{-2}$ in Jul-Sep) and the development index of copepods is the ratio between copepodites stages. See text for details.*

# APPENDIX 3

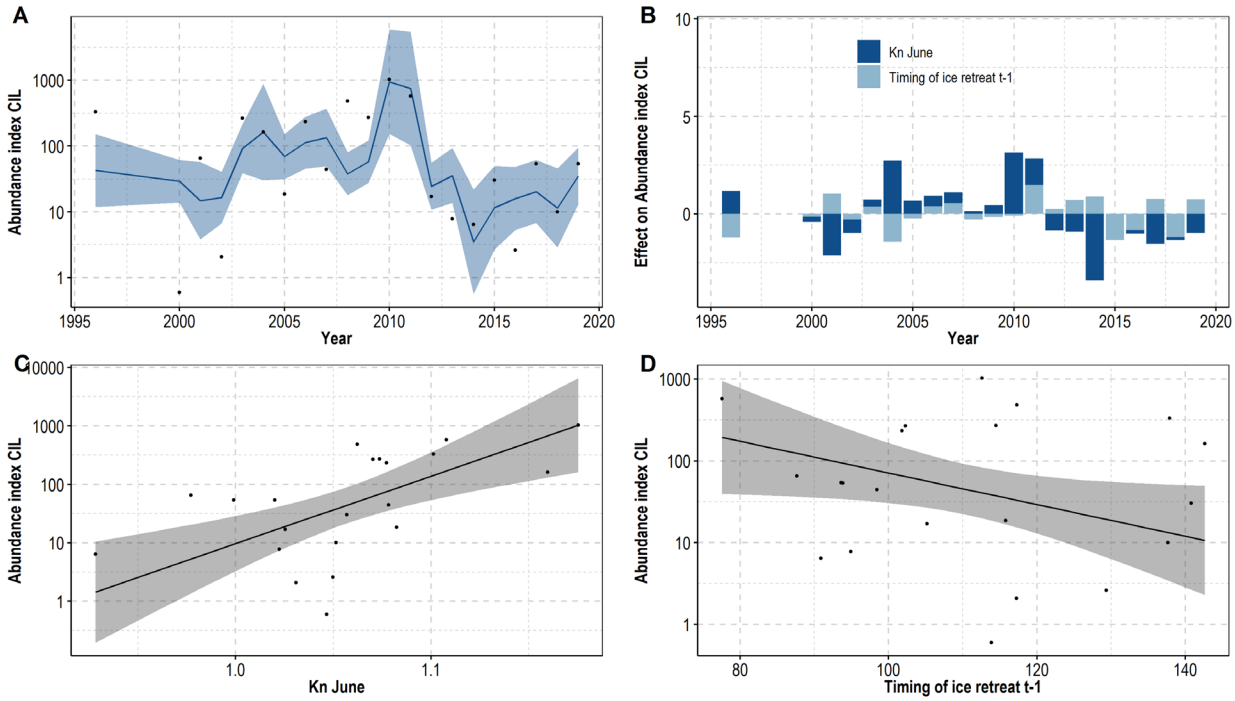


*Figure A.3.1. Selected GAM for capelin abundance index at age 2 in the neGSL (M2): A) Capelin abundance index (black circles) are plotted against GAM predictions (blue line) and the 95% confidence intervals on the predictions (shaded blue area), B) Contribution of each variable to the predicted abundance index every year, C) Effect of Kn in June at age 2 and D) Timing of ice retreat at age 1 on capelin abundance index. Grey areas: 95% confidence intervals.*

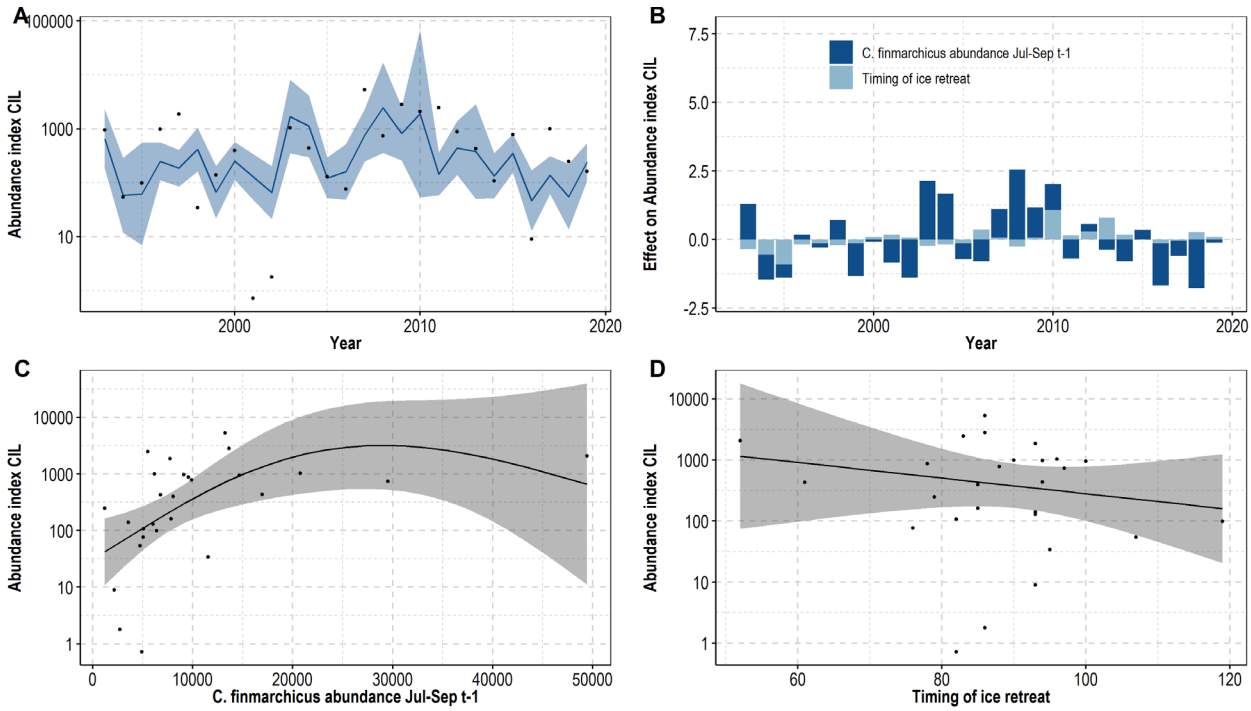


*Figure A.3.2. Selected GAM for capelin abundance index at age 2 in the nwGSL (M2): A) Capelin abundance index (black circles) are plotted against GAM predictions (blue line) and the 95% confidence intervals on the predictions (shaded blue area), B) Contribution of each variable to the predicted abundance index every year, C) Effect of Calanus finmarchicus in July-September at age 1 and D) the timing of ice retreat at age 2 on capelin abundance index. Grey areas: 95% confidence intervals.*

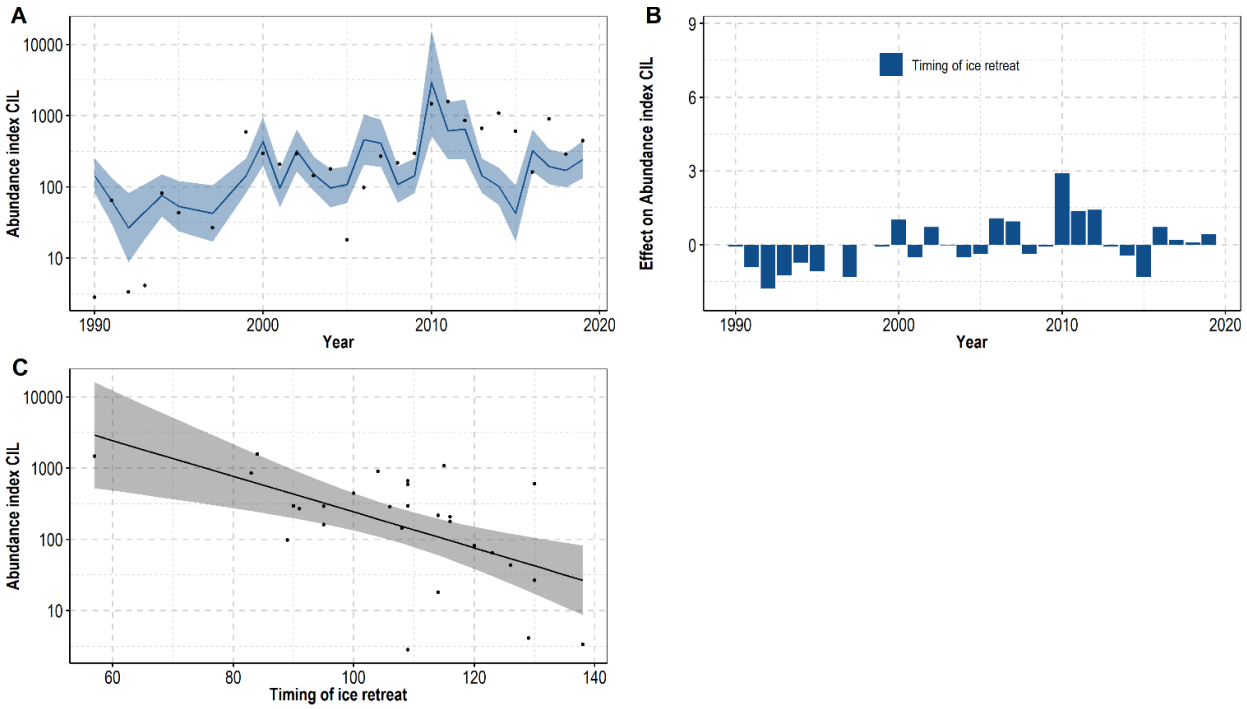


*Figure A.3.3. Selected GAM for capelin abundance index at age 1 in the sGSL (M1): A) Capelin abundance index (black circles) are plotted against GAM predictions (blue line) and the 95% confidence intervals on the predictions (shaded blue area), B) Contribution of each variable to the predicted abundance index every year, C) Effect of the timing of ice retreat at age 1 on capelin abundance index. Grey areas: 95% confidence intervals.*

# APPENDIX 4

*Table A.4.1. Summary of GAMs for capelin Kn of the **neGSL.** Models are sorted by AIC and the head of the table is presented.. Selected models presented in Table 3 are highlighted in grey. The effect of each selected predictor on the response variable can be positive (+), negative (-), bell-shaped (∩) or U-shaped (∪). Non-significant effect are noted with n.s. Models were compared with the AIC when they were fitted on the same time series. The performance of each model is evaluated with the $R^2$, the comparison of deviance explained with bootstrap (* for significantly higher than the distribution obtained by bootstrap and n.s. otherwise) and the Pearson's correlation between predicted and observed values during the Jackknife procedure. Weight is the Akaike weight.*

| Response variables | Years | Predictors | Effect | AIC | ΔAIC | Weight | $R^2$ | Boostrap | Jacknife |
|---|---|---|---|---|---|---|---|---|---|
| K June | 1984-2019 | SST June<br>Timing of ice retreat | -n.s.<br>- | -100.9 | 0.0 | 0.57 | 0.18 | n.s. | 0.16 |
| | | Timing of ice retreat | - | -99.4 | 1.5 | 0.27 | 0.10 | n.s. | 0.11 |
| | | SST June | -n.s | -96.1 | 4.8 | 0.05 | 0.01 | n.s. | -0.12 |
| | 2001-2018 | Timing of ice retreat | -n.s. | -48.0 | 0.0 | 0.12 | 0.13 | n.s. | -0.16 |
| | | SST June<br>Timing of ice retreat | -n.s.<br>-n.s. | -47.3 | 0.7 | 0.09 | 0.20 | n.s. | -0.02 |
| | | SST June<br>*C. hyperboreus* dev. index (early summer) | -n.s.<br>+n.s. | -47.1 | 0.9 | 0.08 | 0.19 | n.s. | 0.12 |
| | | *C. hyperboreus* dev. index (early summer) | +n.s. | -47.0 | 1.1 | 0.07 | 0.08 | n.s. | 0.05 |
| | | SST June | -n.s. | -46.7 | 1.3 | 0.06 | 0.07 | n.s. | 0.01 |
| | | SST June<br>*C. hyperboreus* abundance (early summer) | +n.s.<br>-n.s. | -45.9 | 2.2 | 0.04 | 0.13 | n.s. | 0.10 |

*Table A.4.2. Summary of GAMs for capelin Kn of the **nwGSL.** Models are sorted by AIC and the head of the table is presented. Selected models presented in Table 4 are highlighted in grey. See legend of table A.4.1 for details.*

| Response variables | Years | Predictors | Effect | AIC | ΔAIC | Weight | $R^2$ | Boostrap | Jacknife |
|---|---|---|---|---|---|---|---|---|---|
| K June | 1987-2019 | SST June | -n.s. | -103.9 | 0.0 | 0.27 | 0.02 | n.s. | -0.06 |
| | | Spring timing | +n.s. | -103.8 | 0.1 | 0.26 | 0.01 | n.s. | -0.05 |
| | | Timing of ice retreat | n.s. | -102.5 | 1.4 | 0.14 | -0.03 | n.s. | -0.47 |
| | | SST June<br>Timing of ice retreat | -n.s.<br>n.s. | -101.4 | 2.5 | 0.08 | -0.01 | n.s. | -0.11 |
| | 2003-2018 | Spring timing<br>*C. hyperboreus* abundance (early summer)<br>*C. hyperboreus* dev. index (early summer) | ^<br>-<br>v | -60.3 | 0.0 | 0.27 | 0.74 | * | 0.50 |
| | | Spring timing<br>*C. hyperboreus* abundance (early summer) | ^n.s.<br>- | -58.9 | 1.4 | 0.13 | 0.45 | * | 0.61 |
| | | *C. hyperboreus* abundance (early summer) | -n.s. | -57.8 | 2.6 | 0.08 | 0.19 | n.s. | 0.33 |
| K august (nGSL) | 1995-2019 | SST May-August | n.s. | -71.6 | 0 | 0.37 | -0.01 | n.s. | -0.32 |
| | | Spring timing | n.s. | -70.7 | 0.8 | 0.24 | -0.05 | n.s. | -0.51 |
| | | Timing of ice retreat | n.s. | -70.7 | 0.8 | 0.24 | -0.05 | n.s. | -0.78 |
| | | SST May-August<br>Timing of ice retreat | n.s.<br>n.s. | -68.6 | 3.0 | 0.08 | -0.06 | n.s. | -0.38 |
| | 1995-2019 | *C. hyperboreus* abundance Jul-Sep | n.s. | -67.86 | 0 | 0.19 | 0.03 | n.s. | -0.06 |
| | | SST May-August | n.s. | -67.1 | 0.8 | 0.13 | -0.01 | n.s. | -0.32 |
| | | *C. finmarchicus* abundance Jul-Sep | n.s. | -67.0 | 0.9 | 0.12 | -0.02 | n.s. | -0.19 |

| Response variables | Years | Predictors | Effect | AIC | ΔAIC | Weight | $R^2$ | Boostrap | Jacknife |
|---|---|---|---|---|---|---|---|---|---|
| | | Timing of ice retreat | n.s. | -66.3 | 1.6 | 0.09 | -0.05 | n.s. | -0.78 |
| | | Spring timing | n.s. | -66.2 | 1.6 | 0.08 | -0.05 | n.s. | -0.55 |
| | 2001-2018 | *C. finmarchicus* dev. index (early summer) | - | -65.6 | 0.0 | 0.40 | 0.50 | * | 0.56 |
| | | SST May-August<br>*C. finmarchicus* dev. index (early summer) | n.s.<br>- | -62.7 | 2.9 | 0.10 | 0.49 | * | 0.52 |

*Table A.4.3. Summary of GAMs for capelin Kn of the **sGSL.** Models are sorted by AIC and the head of the table is presented. Selected models presented in Table 5 are highlighted in grey. See legend of table A.4.1 for details.*

| Response variables | Years | Predictors | Effect | AIC | ΔAIC | Weight | $R^2$ | Boostrap | Jacknife |
|---|---|---|---|---|---|---|---|---|---|
| K June | 1986-2019 | Timing of ice retreat | - | -43.8 | 0.0 | 0.48 | 0.23 | n.s. | 0.40 |
| | | SST June<br>Timing of ice retreat | n.s.<br>- | -40.8 | 3.0 | 0.11 | 0.21 | n.s. | 0.1 |
| | 2006-2018 | *C. finmarchicus* dev. index (early summer)<br>*C. hyperboreus* dev. index (early summer) | +<br>+ | -35.3 | 0.0 | 0.98 | 0.97 | * | 0.97 |
| | | *C. hyperboreus* abundance (early summer)<br>*C. finmarchicus* dev. index (early summer)<br>*C. hyperboreus* dev. index (early summer) | +n.s.<br>+<br>+ | -25.8 | 9.5 | 0.01 | 0.97 | * | 0.95 |
| | | *C. hyperboreus* dev. index (early summer) | + | -25.2 | 10.1 | 0.01 | 0.78 | * | 0.84 |
| K september | 1990-2019 | SST May- August | - | -53.4 | 0 | 0.76 | 0.22 | * | 0.34 |
| | | SST May- August<br>Timing of ice retreat | -n.s.<br>n.s. | -50.5 | 2.9 | 0.18 | 0.22 | n.s. | 0.29 |
| | 1999-2019 | *C.finmarchicus* abundance Jul-Sep | + | -52.47 | 0.0 | 0.52 | 0.50 | * | 0.48 |
| | | SST May- August<br>*C.finmarchicus* abundance Jul-Sep | n.s.<br>+ | -49.5 | 3.0 | 0.12 | 0.48 | * | 0.43 |
| | 2001-2018 | *C. finmarchicus* abundance (early summer) | ∩ | -35.3 | 0.0 | 0.27 | 0.53 | * | 0.25 |
| | | *C. finmarchicus* abundance (early summer)<br>*C. hyperboreus* abundance (early summer) | ∩<br>+n.s. | -33.7 | 1.6 | 0.12 | 0.60 | * | 0.30 |
| | | *C. finmarchicus* abundance (early summer)<br>*C. hyperboreus* dev. index (early summer) | ∩<br>+n.s. | -33.5 | 1.8 | 0.11 | 0.56 | * | 0.35 |
| | | *C. hyperboreus* abundance (early summer) | + | -32.8 | 2.5 | 0.08 | 0.44 | * | 0.57 |

*Table A.4.4. Summary of GAMs for capelin abundance at 3 years old (M3) for the **neGSL.** Models are sorted by AIC and the head of the table and key models are presented. Selected models presented in Table 3 are highlighted in grey. See legend of table A.4.1 for details.*

| Response variables | Years | Predictors | Effect | AIC | ΔAIC | Weight | $R^2$ | Boostrap | Jacknife |
|---|---|---|---|---|---|---|---|---|---|
| M3 | 1997-2020 | Larval index t-3<br>Kn June t-1<br>Timing of ice retreat t-2 | -<br>+<br>∩ | 86.3 | 0.0 | 0.62 | 0.58 | * | 0.40 |
| | | Kn June t-1<br>Timing of ice retreat t-2 | +<br>∩ | 88.7 | 2.4 | 0.19 | 0.40 | * | 0.47 |
| | 2004-2020 | Larval index t-3 | n.s. | 75.6 | 0 | 0.32 | 0.26 | n.s. | -0.18 |
| | | Kn June t-1 | +n.s. | 77.7 | 2.0 | 0.12 | 0.10 | n.s. | 0.11 |
| | | Larval index t-3<br>Kn June t-1<br>Timing of ice retreat t-2 | n.s.<br>+n.s.<br>n.s. | 77.9 | 2.3 | 0.1 | 0.52 | * | 0.19 |
| | | Larval index t-3<br>Kn June t-1<br>Timing of ice retreat t-2<br>*Pseudocalanus* abundance in early summer t-3 | -<br>+n.s.<br>∩<br>∪n.s. | 80.7 | 5.1 | 0.03 | 0.60 | * | 0.37 |
| | 1992-2020[1] | Kn June t-1 | | 124.9 | 0 | 0.30 | 0.1 | n.s. | 0.15 |
| | | Kn June t-1<br>Timing of ice retreat t-2 | +n.s.<br>∩n.s. | 125.1 | 0.2 | 0.27 | 0.18 | n.s. | 0.24 |

*Table A.4.5. Summary of GAMs for capelin abundance at 2 years old (M2) for the **neGSL.** Models are sorted by AIC and the head of the table and key models are presented. Selected models presented in Table 3 are highlighted in grey. See legend of table A.4.1 for details.*

| Response variables | Years | Predictors | Effect | AIC | ΔAIC | Weight | $R^2$ | Boostrap | Jacknife |
|---|---|---|---|---|---|---|---|---|---|
| M2 | 1996-2019 | Kn June<br>Timing of ice retreat t-1 | +<br>-n.s. | 87.2 | 0.0 | 0.57 | 0.37 | * | 0.55 |
| | | Kn June | | 88.7 | 1.5 | 0.27 | 0.26 | * | 0.43 |
| | | Larval index t-2<br>Kn June<br>Timing of ice retreat t-1 | n.s.<br>+<br>-n.s. | 90.4 | 3.2 | 0.11 | 0.39 | n.s. | 0.36 |
| | 2003-2019 | Kn June<br>Timing of ice retreat t-1 | +<br>- | 58.9 | 0 | 0.53 | 0.55 | * | 0.72 |
| | | Larval index t-2<br>Kn June<br>Timing of ice retreat t-1 | n.s.<br>+<br>- | 62.3 | 3.3 | 0.1 | 0.61 | * | 0.45 |
| | | Larval index t-2<br>Kn June<br>Timing of ice retreat t-1<br>*Pseudocalanus* abundance early summer t-2 | n.s.<br>+<br>-<br>n.s. | 67.9 | 8.9 | 0.01 | 0.57 | n.s. | 0.31 |
| | 1990-2019[1] | Kn_June<br>Timing of ice retreat t-1 | +<br>-n.s. | 125.0 | 0.0 | 0.36 | 0.24 | * | 0.40 |
| | | Kn_June | + | 125.1 | 0.1 | 0.34 | 0.21 | * | 0.37 |
| | | Kn_June<br>SST June | +<br>n.s. | 127 | 2.2 | 0.13 | 0.22 | * | 0.28 |

*Table A.4.6. Summary of GAMs for capelin abundance at 3 years old (M3) for the **nwGSL.** Models are sorted by AIC and the head of the table and key models are presented. Selected models presented in Table 4 are highlighted in grey. See legend of table A.4.1 for details.*

| Response variables | Years | Predictors | Effect | AIC | ΔAIC | Weight | $R^2$ | Boostrap | Jacknife |
|---|---|---|---|---|---|---|---|---|---|
| M3 | 1997-2020 | Kn June t-1 | ∩ | 71.5 | 0.0 | 0.77 | 0.58 | * | 0.49 |
| | | Kn June t-1<br>Timing of ice retreat t-2 | ∩<br>n.s. | 75.2 | 3.6 | 0.12 | 0.56 | * | 0.47 |
| | | Larval index t-3<br>Kn June t-1<br>Timing of ice retreat t-2 | +n.s.<br>∩<br>n.s. | 76.8 | 5.2 | 0.06 | 0.60 | * | 0.61 |
| | 1995-2019 | Larval index t-3<br>Kn June t-1<br>Timing of ice retreat t-2<br>*Pseudocalanus* abundanceJul-Nov t-3 | n.s.<br>∩.<br>n.s.<br>n.s. | 93.5 | 0 | 0.84 | 0.44 | n.s. | 0.01 |
| | 1992-2020 | Kn June t-1 | ∩ | 98.9 | 0.0 | 0.64 | 0.46 | * | 0.49 |
| | | Kn June t-1<br>Timing of ice retreat t-2 | ∩<br>n.s. | 101.8 | 2.9 | 0.15 | 0.44 | * | 0.47 |

*Table A.4.7. Summary of GAMs for capelin abundance at 2 years old (M2) for the **nwGSL.** Models are sorted by AIC and the head of the table and key models are presented. Selected models presented in Table 4 are highlighted in grey. See legend of table A.4.1 for details.*

| Response variables | Years | Predictors | Effect | AIC | ΔAIC | Weight | $R^2$ | Boostrap | Jacknife |
|---|---|---|---|---|---|---|---|---|---|
| M2 | 1996-2019 | SST May-August | +n.s | 72.0 | 0.0 | 0.43 | 0.15 | n.s. | 0.23 |
| | | Kn_June | +n.s. | 73.3 | 1.3 | 0.22 | 0.09 | n.s. | 0.15 |
| | | Larval index t-2 | -n.s. | 74.9 | 3.0 | 0.10 | 0.00 | n.s. | 0.05 |
| | | Larval index t-2<br>Kn_June<br>Timing of ice retreat t-1 | n.s.<br>+n.s.<br>n.s. | 79.9 | 7.9 | 0.01 | -0.01 | n.s. | 0.01 |
| | 2002-2018 | *C. finmarchicus* abundance (early summer) t-1<br>Timing of ice retreat | +<br>-n.s. | 67.3 | 0.1 | 0.33 | 0.33 | n.s. | 0.27 |
| | | Larval index t-2<br>Kn_June<br>Timing of ice retreat t-1 | n.s.<br>+<br>n.s | 79.9 | 7.9 | 0.26 | -0.01 | n.s. | 0.01 |
| | 1994-2019 | *C. finmarchicus* abundance Jul-Sep t-1<br>Timing of ice retreat | +<br>-n.s. | 83.4 | 0.0 | 0.92 | 0.32 | * | 0.49 |
| | | *C. hyperboreus a*bundance Jul-Sep t-1<br>Timing of ice retreat | n.s.<br>-n.s. | 89.6 | 6.2 | 0.04 | 0.02 | n.s. | 0.03 |
| | | Larval index t-2<br>*C. finmarchicus abundance* Jul-Sep t-1<br>Timing of ice retreat t-1<br>*Pseudocalanus* abundanceJul-Nov t-2 | n.s.<br>+<br>-n.s.<br>n.s. | 90.3 | 6.9 | 0.03 | 0.28 | n.s. | 0.11 |
| | | Larval index t-2<br>Kn June<br>Timing of ice retreat t-1<br>*Pseudocalanus* abundanceJul-Nov t-2 | n.s.<br>+n.s.<br>-n.s.<br>n.s. | 94.6 | 11.2 | 0.00 | 0.02 | n.s. | 0.06 |
| | 1993-2019 | *C. finmarchicus* abundance Jul-Sep t-1<br>Timing of ice retreat | +<br>-n.s. | 118.5 | 0.0 | NA | 0.25 | * | 0.44 |

*Table A.4.8. Summary of GAMs for capelin abundance at 2 years old (M2) for the **sGSL.** Models are sorted by AIC and the head of the table and key models are presented. Selected models presented in Table 5 are highlighted in grey. See legend of table A.4.1 for details.*

| Response variables | Years | Predictors | Effect | AIC | ΔAIC | Weight | $R^2$ | Boostrap | Jacknife |
|---|---|---|---|---|---|---|---|---|---|
| M2 | 1991-2019 | Kn September t-1<br>Timing of ice retreat | -<br>- | 84.6 | 0.0 | 0.49 | 0.59 | * | 0.69 |
| | | SST May-August t-1<br>Timing of ice retreat | +<br>- | 86.3 | 1.6 | 0.22 | 0.57 | * | 0.67 |
| | | Larval index t-2<br>Kn September t-1<br>Timing of ice retreat | -n.s.<br>-<br>- | 87.7 | 3.1 | 0.11 | 0.61 | * | 0.67 |
| | | Larval index t-2<br>SST May-August t-1<br>Timing of ice retreat | n.s.<br>+<br>- | 89.5 | 4.7 | 0.04 | 0.57 | * | 0.63 |
| | 2001-2019 | *C. finmarchicus* abundanceJul-Nov t-1<br>Timing of ice retreat | -n.s.<br>-n.s. | 60.3 | 0.0 | 0.7 | 0.29 | n.s. | 0.19 |
| | | Larval index t-2<br>Kn September t-1<br>Timing of ice retreat<br>*Pseudocalanus* abundanceJul-Nov t-2 | n.s.<br>-<br>-n.s.<br>n.s. | 62.9 | 2.6 | 0.19 | 0.46 | n.s. | 0.28 |

*Table A.4.9. Summary of GAMs for capelin abundance at 1 year old (M1) for the **sGSL.** Models are sorted by AIC and the head of the table and key models are presented. Selected models presented in Table 5 are highlighted in grey. See legend of table A.4.1 for details.*

| Response variables | Years | Predictors | Effect | AIC | ΔAIC | Weight | $R^2$ | Boostrap | Jacknife |
|---|---|---|---|---|---|---|---|---|---|
| M1 | 1990-2019 | Timing of ice retreat | - | 105.7 | 0.0 | 0.72 | 0.31 | * | 0.47 |
| | | Larval index t-1<br>Timing of ice retreat | +n.s.<br>- | 107.6 | 1.9 | 0.27 | 0.31 | * | 0.45 |
| | | Larval index t-1 | +n.s. | 116.1 | 10.4 | 0.00 | 0.00 | n.s | 0.01 |
| | 2000-2019 | Larval index t-1<br>Timing of ice retreat<br>*Pseudocalanus* abundance Jul-Nov t-1 | n.s.<br>-n.s.<br>+n.s. | 68.3 | 5.2 | NA | 0.05 | n.s. | 0.03 |